SLAC–PUB–5447
September 1991
(T/E)

RESONANT SUBSTRUCTURE IN $\overline{K}\pi\pi\pi$ DECAYS OF D MESONS*

D. Coffman,[a] F. DeJongh,[b] G. P. Dubois,
G. Eigen, D. G. Hitlin, C. G. Matthews, A. Mincer,[c]
J. Richman,[d] A. J. Weinstein, W. J. Wisniewski, Y. Zhu[e]

California Institute of Technology, Pasadena, CA 91125

T. Bolton,[f] K. O. Bunnell, R. E. Cassell, D. H. Coward, P. C. Kim,[a]
J. Labs, A. Odian, D. Pitman,[g] R. H. Schindler, W. Toki, S. Wasserbaech[h]

Stanford Linear Accelerator Center, Stanford, CA 94305

J. J. Drinkard,[i] C. Gatto,[j] C. A. Heusch, W. S. Lockman,
M. Scarlatella, H. F. W. Sadrozinski, T. L. Schalk, A. Seiden, S. Weseler[k]

University of California at Santa Cruz, Santa Cruz, CA 95064

B. I. Eisenstein, T. Freese,[l] G. Gladding,
J. M. Izen, I. E. Stockdale,[m] B. Tripsas[n]

University of Illinois at Urbana-Champaign, Urbana, IL 61801

U. Mallik, M. Z. Wang

University of Iowa, Iowa City, IA 52242

J. Brown, T. H. Burnett, A. D. Li, R. Mir,[o]
P. M. Mockett, B. Nemati,[p] L. Parrish, H. Willutzki[q]

University of Washington, Seattle, WA 98195

The Mark III Collaboration

Submitted to *Physical Review D.*

* Work supported by Department of Energy contracts DE-AC03-76SF00515, DE-AC02-76ER01195, DE-AC03-81ER40050, DE-AC02-87ER40318, and DE-AM03-76SF00010; and also by the National Science Foundation.

a. Present address: Wilson Laboratory, Cornell University, Ithaca, NY 14853.

b. Present address: Fermilab, PO Box 500, Batavia, IL 60510.

c. Present address: New York University, New York City, NY 10003.

d. Present address: University of California at Santa Barbara, Santa Barbara, CA 93106.

e. Present address: International Telephone and Teledata, Inc., PO Box 80160, Goleta, CA 93118.

f. Present address: Columbia University, PO Box 137, Irvington, NY 10533.

g. Present address: University of Victoria, Victoria, BC V8W 3P6 Canada.

h. Present address: EP Division, CERN, 1211 Geneva 23, Switzerland.

i. Present address: Centre de Physique des Particules de Marseille, F-13288 Marseille, CEDEX 9, France.

j. Present address: INFN, 80125 Napoli, Italy.

k. Present address: University of Karlsruhe, Postfach 6980, D-7500 Karlsruhe, Germany.

l. Present address: Systems Control Technology, 2300 Geng Road, Palo Alto, CA 94303.

m. Present address: NASA Ames Research Center, MS 258-6, Moffett Field, CA 94035.

n. Present address: Center for Naval Analyses, 4401 Ford Avenue, Alexandria, VA 22302.

o. Present address: Indiana University, Bloomington, IN 47405.

p. Present address: State University of New York at Albany, Albany, NY 12222.

q. Present address: Brookhaven National Laboratory, Upton, NY 11973.

ABSTRACT

We determine the resonant substructure of $D \to \overline{K}\pi\pi\pi$ decays, extracting the relative fractions and phases of the amplitudes contributing to the $K^-\pi^+\pi^+\pi^-$, $\overline{K}^0\pi^+\pi^+\pi^-$, $K^-\pi^+\pi^+\pi^0$ and $\overline{K}^0\pi^+\pi^-\pi^0$ final states. We find that two-body decay modes account for at least 75% of these decays. We obtain branching ratios for $D \to \overline{K}a_1(1260)$, $D \to \overline{K}^*\rho$, $D \to \overline{K}_1(1270)\pi$, $D \to \overline{K}_1(1400)\pi$ and $D^0 \to \overline{K}^0\omega$ decay modes, as well as for several three- and four-body decay modes. In the case of $D \to \overline{K}a_1(1260)$ and $D \to \overline{K}^*\rho$, we obtain the branching ratios for all three possible isospin combinations, enabling us to extract the isospin 1/2 and 3/2 amplitudes, and their relative phases. We find that the isospin 3/2 amplitudes are suppressed relative to the isospin 1/2 amplitudes. This implies that the widths of the D^+ modes are suppressed relative to those of the D^0, confirming that an understanding of the lifetime difference of the D^0 and D^+ depends on an understanding of two-body hadronic decays.

For the $D \to \overline{K}^*\rho$ decay modes, we obtain detailed information on the polarization of the $\overline{K}^*$ and ρ. This enables us to place constraints on the form factors for $D \to \overline{K}^*$ and $D \to \rho$ transitions. A comparison of our results on $D \to \overline{K}^*\rho$ decays with recent results on semileptonic decays allows us to test the factorization hypothesis.

I. INTRODUCTION

A large number of exclusive hadronic final states have been observed for the D mesons, accounting for nearly all of their total hadronic widths [1,2]. In most cases, these final states contain two, three, or four long-lived particles [3]. Detailed studies of three-particle final states [4-7] have shown these to be dominated by two-body decay modes in which the final state is produced by the decay of a broad intermediate resonance.

Measurements of the lifetimes of the charmed mesons [8] show that the lifetime of the D^+ is 2.5 ± 0.1 times that of the D^0. The ratio of the hadronic widths, obtained by subtracting the measured semileptonic widths [9] from the total widths of the D^0 and D^+, is

$$\frac{\Gamma_H(D^0)}{\Gamma_H(D^+)} = 3.2 \pm 0.2 \quad . \tag{1}$$

The ratio of hadronic widths of the modes $D \to \overline{K}\pi$, $\overline{K}\rho$, and $\overline{K}^*\pi$, which account for 30% and 23% of the total hadronic widths of the D^0 and D^+ and have been measured in all isospin combinations, is [10]:

$$\frac{\Gamma(D^0 \to K^-\pi^+, \overline{K}^0\pi^0, K^-\rho^+, \overline{K}^0\rho^0, K^{*-}\pi^+, \overline{K}^{*0}\pi^0)}{\Gamma(D^+ \to \overline{K}^0\pi^+, \overline{K}^0\rho^+, \overline{K}^{*0}\pi^+)} = 4.0 \pm 1.0 \quad . \tag{2}$$

This suggests that an understanding of the lifetime ratio requires an understanding of two-body decays. The $\overline{K}\pi\pi\pi$ final states for which branching fractions have been measured account for 40% and 20% of the total hadronic widths of the D^0 and D^+. We are therefore motivated to determine whether these final states are also dominated by two-body decay modes whose patterns of branching fractions also match the ratio of the total hadronic widths.

We present herein an analysis of the resonant substructure of the following final states:

$$
\begin{aligned}
D^0 &\to K^-\pi^+\pi^+\pi^- \quad , \\
D^+ &\to \overline{K}^0\pi^+\pi^+\pi^- \quad , \\
D^+ &\to K^-\pi^+\pi^+\pi^0 \quad , \\
D^0 &\to \overline{K}^0\pi^+\pi^-\pi^0 \quad .
\end{aligned}
\tag{3}
$$

This analysis is the first detailed study of a four-particle final state [11]. We show that two-body decays are the principal component, and obtain branching fractions of decays to two vector mesons (VV), to a pseudoscalar and an axial vector meson (PA), and to nonresonant decay modes.

Table I describes the relative branching fractions of various two-body decay modes to four-particle final states. Each of these decay modes has three isospin combinations. The amplitudes for decays such as these, for which one of the mesons has isospin $1/2$ and the other isospin 1, can be written in terms of isospin $1/2$ and $3/2$ components:

$$
\begin{aligned}
A(D^+ \to |+\frac{1}{2};+1\rangle) &= \sqrt{3}A_{3/2}e^{i\delta_{3/2}} \quad , \\
A(D^0 \to |-\frac{1}{2};+1\rangle) &= \sqrt{\frac{1}{3}}\left(A_{3/2}e^{i\delta_{3/2}} + \sqrt{2}A_{1/2}e^{i\delta_{1/2}}\right) \quad , \\
A(D^0 \to |+\frac{1}{2};\ \ 0\rangle) &= \sqrt{\frac{1}{3}}\left(\sqrt{2}A_{3/2}e^{i\delta_{3/2}} - A_{1/2}e^{i\delta_{1/2}}\right) \quad .
\end{aligned}
\tag{4}
$$

If the widths for all three isospin combinations are known, the ratio $|A_{1/2}/A_{3/2}|$ and the difference $\delta_{1/2}-\delta_{3/2}$ can be calculated. This decomposition has been performed [6] for $D \to \overline{K}\pi$, $\overline{K}\rho$, and $\overline{K}^*\pi$. The ratios of isospin amplitudes $|A_{1/2}/A_{3/2}|$ for all three modes are ~ 3.5. The isospin phase shifts can be sizeable. A further goal of this analysis is to perform the isospin decomposition for new modes.

The matrix element for a semileptonic decay may be factorized into a leptonic current and a hadronic current:

$$
A(D \to M\bar{\ell}\nu) = \frac{G_F}{\sqrt{2}}V_{cq}L^\mu H_\mu \quad , \tag{5}
$$

where V_{cq} is the Cabibbo–Kobayashi–Maskawa (CKM) matrix element, L^μ is the leptonic current

$$L^\mu = \ell\gamma^\mu(1-\gamma^5)\nu \quad , \tag{6}$$

and H_μ is the hadronic current

$$H_\mu = \langle M|J_\mu|D\rangle \quad . \tag{7}$$

Motivated by the spectator model of two-body hadronic weak decays, one may make the factorization assumption:

$$A(D \to Mm) = \frac{G_F}{\sqrt{2}} V_{cq} h^\mu H_\mu \quad . \tag{8}$$

Here, H_μ is the same as in Equation (7), and the current h_μ is

$$h^\mu = \langle m|J^\mu|0\rangle \quad , \tag{9}$$

which is proportional to the decay constant of the meson m.

In the model of Bauer, Stech, and Wirbel (BSW) [12], the amplitude in Equation (8) has two terms: one is proportional to the quantity a_1 ($\sim$ 1.2), which parametrizes the strength of external W-emission, e.g. $D^0 \to K^-\pi^+$, and the other is proportional to the parameter a_2 (~ -0.5), which parametrizes the strength of internal W-emission, e.g. $D^0 \to \overline{K}^0\pi^0$. Thus, internal W-emission decays are expected to be suppressed relative to external W-emission decays; however, they may be greatly enhanced by isospin phase shifts as in Equation (4). Cabibbo-allowed D^+ decays such as $D^+ \to \overline{K}^0\pi^+$ proceed via both internal and external W-emission. In the BSW model, it is destructive interference between these processes which accounts for the reduced D^+ hadronic width. The BSW predictions which we will test are [14]:

$$
\begin{aligned}
B(D^+ \rightarrow \overline{K}^{*0}\rho^+) &= 17\% \quad , \\
B(D^0 \rightarrow K^{*-}\rho^+) &= 21\% \quad , \\
B(D^0 \rightarrow \overline{K}^{*0}\rho^0) &= 2.5\% \quad , \\
B(D^+ \rightarrow \overline{K}^0 a_1(1260)^+) &= 3.8\% \quad , \\
B(D^0 \rightarrow K^- a_1(1260)^+) &= 1.5\% \quad , \\
B(D^0 \rightarrow \overline{K}^0 a_1(1260)^0) &= 0\% \quad .
\end{aligned}
\tag{10}
$$

The factorization assumption in the BSW model does not allow for isospin phase shifts different from zero, in contradiction to experiment. However, if we measure the branching fractions to all three isospin combinations and perform the isospin decomposition we can calculate the effect of the isospin phase shifts and therefore make an improved comparison of the data to the predictions.

If the factorization assumption is valid, results from semileptonic decays should apply to hadronic decays. The matrix element for the decay $D^+ \rightarrow \overline{K}^{*0}e^+\nu$ has been studied in detail by the E691 Collaboration [15]. The results should apply to the decay modes $D \rightarrow \overline{K}^*\rho$. Thus, by comparing our results on $D \rightarrow \overline{K}^*\rho$ to the semileptonic results, we can test the factorization hypothesis.

II. EVENT SELECTION

The data, a total of 9.56 pb^{-1}, were collected at the peak of the $\psi(3770)$ resonance with the Mark III detector [19] at the SLAC e^+e^- storage ring SPEAR. At the $\psi(3770)$, D mesons are produced in the reaction $e^+e^- \rightarrow \psi(3770) \rightarrow D\bar{D}$. This analysis uses information from the drift chamber, time of flight system, and electromagnetic calorimeter. The drift chamber has an acceptance of 84% for charged particles. The time of flight system provides π/K discrimination up to 1.2 GeV/c at 2σ separation. The lead-gas electromagnetic calorimeter is located inside the magnet

coil, has a 94% geometric acceptance, and is fully efficient for photons with energy above 0.1 GeV.

The event selection procedures are described in detail in References 11, 16, and 17. We briefly summarize the main features here. Charged tracks are classified as pions or kaons with the time of flight system or with dE/dx information from the drift chamber. Neutral kaons are detected through the decay $\overline{K}^0 \to K^0_S \to \pi^+\pi^-$. Candidate $\pi^+\pi^-$ pairs are kinematically constrained to the $\overline{K}^0$ mass. For the $D^+ \to \overline{K}^0\pi^+\pi^+\pi^-$ final state, all K^0_S candidates are used. For the $D^0 \to \overline{K}^0\pi^+\pi^-\pi^0$ final state, in order to improve the signal to noise ratio, the $\pi^+\pi^-$ vertex is required to be more than 3 mm from the beam axis, and the vertex position and K^0_S momentum vector are required to align in the xy-plane.

Neutral pion candidates are detected through the decay $\pi^0 \to \gamma\gamma$. The $\gamma\gamma$ pair is kinematically constrained to the π^0 mass. The fitted photon energies are required to be greater than 0.05 GeV. The cosine of the angle between the photon direction and that of the nearest charged track must be less than 0.95 at the entrance to the calorimeter. For the $D^+ \to K^-\pi^+\pi^+\pi^0$ final state, the cosine of the π^0 decay angle is required to be less than 0.7, where the π^0 decay angle is defined as the angle between the direction of one of the photons in the π^0 rest frame and the direction of the laboratory frame.

Finally, for the $D^+ \to K^-\pi^+\pi^+\pi^0$ final state, we require that there be less than two additional isolated showers in the event, where an isolated shower is defined as a neutral shower whose measured energy is greater than 0.08 GeV and for which the cosine of the angle to the nearest charged track is less than 0.97 at the entrance to the shower counter. The efficiency of this requirement can be obtained directly using

the Mark III sample of 1600 $D^+ \to K^-\pi^+\pi^+$ events. By measuring the fraction of these events which pass this requirement, we obtain an efficiency of 0.549 ± 0.028.

For each $\overline{K}\pi\pi\pi$ combination, an effective recoil mass can be calculated using $E_{\rm recoil} = E_{\psi(3770)} - E_{\overline{K}\pi\pi\pi}$ and $P_{\rm recoil} = -P_{\overline{K}\pi\pi\pi}$. For a real $D \to \overline{K}\pi\pi\pi$ event, both the invariant mass and the recoil mass of the $\overline{K}\pi\pi\pi$ combination will be near the D mass. For each $\overline{K}\pi\pi\pi$ combination, we perform a kinematic fit in which the mass of the combination is constrained to the D mass and the recoil mass is allowed to vary. The signal can then be seen in the recoil mass plot as a peak at the D mass. With this type of constraint, all events have the same amount of phase space for the decay throughout the recoil mass plot. This has the advantage that the kinematic boundaries of the phase space for the four-body decay are the same in the sideband regions and the signal regions of the recoil mass plot. The recoil mass plot is fitted with a Gaussian for the signal and a polynomial with an error function cutoff at high mass for the background.

The recoil mass plot for the $D^0 \to K^-\pi^+\pi^+\pi^-$ final state is shown in Figure 1(a). There are 1281 ± 45 events above background. The branching fraction has been determined previously by Mark III to be $(9.1 \pm 0.8 \pm 0.8)\%$ [18].

The recoil mass plot for the $\overline{K}^0\pi^+\pi^+\pi^-$ final state is shown in Figure 1(b). There are 209 ± 20 events above background. The branching fraction has been determined previously by Mark III to be $B(D^+ \to \overline{K}^0\pi^+\pi^+\pi^-) = (6.6 \pm 1.5 \pm 0.5)\%$ [18].

The recoil mass plot for the $K^-\pi^+\pi^+\pi^0$ final state is shown in Figure 1(c). There are 142 ± 20 events above background. We obtain $B(D^+ \to K^-\pi^+\pi^+\pi^0) = (5.8 \pm 1.2 \pm 1.2)\%$. This value is determined using the cross-section in Reference 18 and supercedes the value in Reference 17. It is in agreement with the E691 value $B(D^+ \to K^-\pi^+\pi^+\pi^0) = (6.3 \pm 1.3 \pm 1.5)\%$ [20].

The recoil mass plot for the $\overline{K}^0\pi^+\pi^-\pi^0$ final state is shown in Figure 1(d). There are 140 ± 28 events above background. We obtain $B(D^0 \to \overline{K}^0\pi^+\pi^-\pi^0) = (10.3 \pm 2.2 \pm 2.5)\%$, which is a new result.

III. THE LIKELIHOOD FUNCTION

For each $D \to \overline{K}\pi\pi\pi$ final state, there are several two-body and three-body decay modes which can contribute. We determine the contribution of each decay mode using a maximum likelihood fit. The fitting technique is a straightforward extension of the techniques commonly used in three-body Dalitz plot fits. For each decay mode, we define a complex amplitude in the four-body phase space. These amplitudes overlap and interfere. We define a probability density function (p.d.f.) which consists of a coherent sum of these amplitudes, and fit to the data to determine the relative fractions and phases of these amplitudes.

The p.d.f., a function in the phase space defined by the four-momenta of the decay products of the D candidate, provides a complete description of the decay in the five-dimensional phase space. A wide variety of kinematic variables can be defined, such as two- and three-body invariant masses, and helicity angles. Since we are analyzing the complete phase space, and not projections, we do not have to "choose" any five particular variables, but instead use whichever ones are convenient for each term in the p.d.f.

The likelihood function $\mathcal{L}$ is defined as

$$\mathcal{L} = \prod_{events} \mathcal{F} \quad , \tag{11}$$

where $\mathcal{F}$ is the p.d.f. The p.d.f. consists of a signal term $\mathcal{F}_S$ and a background term $\mathcal{F}_B$:

$$\mathcal{F} = \frac{R_{S/B}\mathcal{F}_S + \mathcal{F}_B}{R_{S/B} + 1} \quad . \tag{12}$$

For each event we calculate the ratio of signal to background, $R_{S/B}$, as a function of recoil mass, using the curve fitted to the recoil mass plot.

The signal p.d.f., $\mathcal{F}_S$, consists of a coherent sum of complex amplitudes, weighted by the density of states in phase space and the detector efficiency. Each amplitude is individually normalized over phase space before taking into account detector efficiency, and $\mathcal{F}_S$ as a whole is normalized over phase space weighted by the detector efficiency:

$$\begin{aligned} \mathcal{F}_S &= \frac{1}{N_{\mathcal{F}_S}} \epsilon \left| \sqrt{f_1^M}\, e^{i\alpha_1} \frac{S_1}{\sqrt{N_1}} + \ldots + \sqrt{f_n^M}\, e^{i\alpha_n} \frac{S_n}{\sqrt{N_n}} \right|^2 \phi \\ &= \frac{1}{N_{\mathcal{F}_S}} \sum_{i=1}^{n} \sum_{j=1}^{n} \sqrt{f_i^M} \sqrt{f_j^M}\, \Re e \left(e^{i(\alpha_i - \alpha_j)} \frac{\epsilon S_i S_j^* \phi}{\sqrt{N_i N_j}} \right) \quad . \end{aligned} \tag{13}$$

The S_i are complex amplitudes varying over phase space; ϵ is the detector efficiency as a function of location in phase space; ϕ is the four-body phase space function; N_i are the normalizations of the amplitudes over phase space weighted by ϕ; and $N_{\mathcal{F}_S}$ is the overall normalization of the p.d.f. The fractions f_i^M and the phases α_i are varied in the fit to maximize the likelihood.

The background p.d.f. is:

$$\mathcal{F}_B = \frac{1}{N_{\mathcal{F}_B}} \sum_{i=1}^{m} g_i^M \frac{\epsilon B_i \phi}{M_i} \quad . \tag{14}$$

The B_i are functions which describe the resonant content of the background. They are similar to the S_i, except they do not interfere with each other. The fractions g_i^M

are allowed to vary in the fit. The normalizations M_i and $N_{\mathcal{F}_B}$ are evaluated with the same procedures used for $\mathcal{F}_S$.

To find the maximum of the likelihood function, we minimize $-\ell n\,\mathcal{L}$. The functions ϵ and ϕ do not depend on the f_i^M, g_i^M, or α_i, and are factored out before the minimization. If we define $\mathcal{F}_S = \epsilon\phi S$ and $\mathcal{F}_B = \epsilon\phi B$, then

$$-\ell n\,\mathcal{L} = -\sum_{\textit{signal events}} \ell n \left(\frac{R_{S/B}S + B}{R_{S/B}+1} \right) - \ell n\,\epsilon\phi \quad . \tag{15}$$

The term $\ell n\,\epsilon\phi$ is a constant for the purpose of minimizing F and is neglected. We therefore never explicitly need to evaluate ϵ and ϕ; they are taken into account entirely by Monte Carlo techniques in the normalization procedure.

The minimization is performed by setting one fraction and one phase to a constant and letting the relative fractions and phases vary. However $\mathcal{F}_P$, the p.d.f. for the produced distribution of events before efficiency effects, must be normalized to one. This function is:

$$\mathcal{F}_P = \left| \sqrt{f_1^M}\, e^{i\alpha_1} \frac{S_1}{\sqrt{N_1}} + \ldots + \sqrt{f_n^M}\, e^{i\alpha_n} \frac{S_n}{\sqrt{N_n}} \right|^2 \phi \quad . \tag{16}$$

To properly normalize $\mathcal{F}_P$ we rescale the fractions f_i^M to obtain the physical fractions f_i:

$$f_i = \frac{f_i^M}{P} \quad , \tag{17}$$

where P is the integral of $\mathcal{F}_P$:

$$P = \sum_{i=1}^{n}\sum_{j=1}^{n} \sqrt{f_i^M}\sqrt{f_j^M}\, \Re e \left(e^{i(\alpha_i - \alpha_j)} N_{ij} \right) \quad , \tag{18}$$

and N_{ij} is the overlap integral of the ith and jth amplitudes. Note that due to interference between the amplitudes,

$$\sum_{i=1}^{n} f_i \neq 1 \quad . \tag{19}$$

The final states $D^0 \to K^-\pi^+\pi^+\pi^-$, $D^+ \to \overline{K}^0\pi^+\pi^+\pi^-$, and $D^+ \to K^-\pi^+\pi^+\pi^0$ all have two identical positive pions. The $\pi^+\pi^-$ or $\pi^+\pi^0$ combination with the higher mass is referred to as $(\pi^+\pi^-)_{\rm high}$ or $(\pi^+\pi^0)_{\rm high}$, the other as $(\pi^+\pi^-)_{\rm low}$ or $(\pi^+\pi^0)_{\rm low}$. The $\overline{K}^0\pi^+$ or $K^-\pi^+$ combination formed with the π^+ not used in $(\pi^+\pi^-)_{\rm high}$ or $(\pi^+\pi^0)_{\rm high}$ is referred to as $(\overline{K}^0\pi^+)_1$ or $(K^-\pi^+)_1$, the other as $(\overline{K}^0\pi^+)_2$ or $(K^-\pi^+)_2$. Alternatively, phase space may be divided according to high and low $\overline{K}\pi^+$ mass, with the notation $(K^-\pi^+)_{\rm high}$, $(\pi^+\pi^-)_1$, etc.

For the $D^0 \to \overline{K}^0\pi^+\pi^-\pi^0$ final state, the charged pions are not identical. Ideally, mass plots involving the charged pions would be divided according to the charge of the pion relative to the charge of the charmed quark. However, the charge of the charmed quark cannot be determined for events in this final state as reconstructed in this analysis. Therefore, we continue to divide plots the same way as for the other final states, as if the charged pions were identical. For example, we will refer to $(\pi^\pm\pi^0)_{\rm high}$ and $(\overline{K}^0\pi^\mp)_1$.

For the final states with identical pions, the amplitudes are symmetrized. Therefore, parametrizing the phase space in terms of high and low mass combinations has no impact on the p.d.f., but is done simply for our convenience. Nonetheless, $(K^-\pi^+)_1$ and $(K^-\pi^+)_2$, for example, are independent kinematic variables; plotting them separately provides more information than a histogram with two entries per event. The $\overline{K}^*$ peaks from two different amplitudes may have different heights in the different $K^-\pi^+$ plots.

We model each decay chain with a complex amplitude consisting of a Breit-Wigner propagator for each resonance in the decay chain, multiplied by a form factor

for each vertex in the decay chain and a matrix element depending on the spin and parity of the intermediate resonances and final decay products. These matrix elements are evaluated in the Lorentz invariant [21] or helicity amplitude [22] formalism.

Lorentz invariant matrix elements are constructed by describing a decay in terms of sequential two-body vertices. Intermediate states may consist of resonances, or nonresonant states in which two particles are in a particular partial wave. The total matrix element is the product of the matrix elements for each vertex, which are constructed from the four-momenta and polarization vectors of the incoming and two outgoing states. The Lorentz invariant matrix elements used are listed in Table II.

The decay $D \rightarrow VV$ may be described in terms of three helicity amplitudes. Alternatively, it may also be described in terms of amplitudes for the three possible partial waves, S, P, or D. These two bases each form a complete basis for VV decays.

The helicity formalism leads to three amplitudes $A_{1,1}$, $A_{-1,-1}$, and $A_{0,0}$. The measurement of longitudinal polarization of the K^* in semileptonic D decays [23] suggests that we fit the transverse amplitudes $A_{1,1}, A_{-1,-1}$ independently from the longitudinal amplitude, $A_{0,0}$.

We define the transverse amplitude as:

$$\begin{aligned} A_T &= A_{1,1} + A_{-1,-1} \\ &= -\sin\theta_1 \sin\theta_2 \cos\phi \quad , \end{aligned} \tag{20}$$

and the longitudinal amplitude as:

$$\begin{aligned} A_L &= A_{0,0} \\ &= \cos\theta_1 \cos\theta_2 \quad , \end{aligned} \tag{21}$$

where θ_1 and θ_2 are the helicity angles of the two vector mesons, and ϕ is the angle between their decay planes. These decay planes are defined by the direction of the vector meson and one of its decay products, measured in the D rest frame. In the case

of $D \to \overline{K^*}\rho$, the helicity angle of the $\overline{K^*}$ is defined as the angle between the D and the kaon measured in the $\overline{K^*}$ rest frame; the helicity angle of the ρ is defined as the angle between the D and the π^- or π^0 measured in the ρ rest frame; the orientation of the decay plane of the ρ is defined by

$$\vec{p}(\pi^+) \times \vec{p}(\pi^{0,-}) \tag{22}$$

and that of the $\overline{K^*}$ by

$$\vec{p}(\pi) \times \vec{p}(K) \quad . \tag{23}$$

The $l = 1$ amplitude, in the helicity formalism, is:

$$\begin{aligned} A_{l=1} &= A_{1,1} - A_{-1,-1} \\ &= \sin\theta_1 \sin\theta_2 \sin\phi \quad . \end{aligned} \tag{24}$$

If the three amplitudes, A_T, A_L, and $A_{l=1}$ are included in a fit, then any possible helicity state can be modeled. With our definitions of the helicity angles and the angle ϕ, we have, in the nonrelativistic limit:

$$A_{l=0} = -A_T + A_L \quad , \tag{25}$$

$$A_{l=2} = -\sqrt{1/6}A_T - \sqrt{4/6}A_L \quad . \tag{26}$$

When Lorentz invariant matrix elements are used, a relativistic Breit–Wigner propagator [24] is included for each intermediate resonance:

$$\frac{-1}{m^2 - m_0^2 + i\Gamma m_0} \quad . \tag{27}$$

If the helicity formalism is being used, only the angular distribution information is included in the matrix element, and the momentum dependencies must be put in by hand. In this case, the following Breit–Wigner propagator is used:

$$\frac{-\sqrt{\Gamma m/p_{cm}}}{m^2 - m_0^2 + i\Gamma m_0} \quad . \tag{28}$$

The decay chains used, corresponding to the amplitudes in Table II, are shown in Table III. Tables II and III, combined with the equations in this section, provide the information necessary to reproduce our results in a Monte Carlo generator.

A very large number of decay modes can contribute to each final state; it is not practical to perform a fit that includes all possible decay modes simultaneously. Instead, we perform a number of fits assuming different combinations of partial waves and two-body decay modes. Only the lowest available partial waves yield significant contributions, and the fractions of two-body amplitudes and the four-body nonresonant amplitude remain consistent among the best fits. Nonresonant $\overline{K}^*\pi\pi$ and $\overline{K}\rho\pi$ amplitudes also contribute. The fits are not always sensitive to the partial wave content of these three-body amplitudes; nevertheless the overall fractions remain consistent among the best fits.

Except for the very broad $a_1(1260)$ Breit–Wigner propagator, The $\overline{K}a_1(1260)$ amplitudes are identical to the amplitudes for nonresonant $\overline{K}\rho\pi$ in which the ρ and π are in a relative S-wave. Fits in which both of these amplitudes are included do not result in a significantly better likelihood; however, the fractions for each of these two amplitudes become highly uncertain, while their combined fraction remains well determined. This occurs because the relative phases for these amplitudes adjust so that there is nearly maximum constructive or destructive interference to an extent that depends very sensitively on the conditions of each particular fit. A systematic uncertainty for this effect would be both very large and difficult to quantify. Therefore, we make the assumption that the amplitude for nonresonant $\overline{K}\rho\pi$ in which the ρ and π are in a relative S-wave is zero, and do not include any systematic uncertainties for its possible existence. Nevertheless, we retain the *caveat* that the presence of this one

nonresonant amplitude can have a large effect on the fraction of $\overline{K}a_1(1260)$, only if its phase is adjusted to produce strong interference. We find that this assumption is well justified: Fits in which the $\overline{K}a_1(1260)$ amplitudes are replaced by the three-body amplitude result in a significantly poorer likelihood, with a difference in $(-\ell n\,\mathcal{L})$ of at least 15. Also, the fractions of $\overline{K}\rho\pi$ in other partial waves are relatively small. We assume 1.26 GeV/c^2 for the mass of the $a_1(1260)$, and 0.4 GeV for the width [25]. We include in the systematic uncertainties the effect of varying the mass between 1.2 and 1.3 GeV/c^2, and the width between 0.3 and 0.5 GeV.

We estimate the systematic errors on the fractions by varying the partial waves of the three-body amplitudes, the event-selection criteria, the background parametrization, the parametrizations of the amplitudes, the parameters of the intermediate resonances, the detector resolution, Monte Carlo statistics, and the possible presence of additional amplitudes.

Amplitudes which do not yield significant contributions remain small in all fits with good likelihood. We can therefore set meaningful upper limits. In addition to including the statistical errors in the calculation of the limit, we include any systematic variations in the fractions obtained in different fits.

IV. RESULTS FOR EACH FINAL STATE

The $D^0 \to K^-\pi^+\pi^+\pi^-$ final state has the highest statistics and the lowest background of the final states studied in this analysis. The $D^+ \to \overline{K}^0\pi^+\pi^+\pi^-$ and $D^+ \to K^-\pi^+\pi^+\pi^0$ final states have lower statistics, and somewhat higher background. Since the resonant substructure is expected to be relatively simple in these two final states, it is still possible to extract statistically significant results. Furthermore, some decay modes contribute to both of these final states, allowing cross-checks between the analyses. Although the $D^0 \to \overline{K}^0\pi^+\pi^-\pi^0$ final state suffers from still

lower statistics and higher background, the analysis of this final state is required in order to provide information about the third isospin combination of many decay modes, allowing us to complete the pattern for these modes. The sensitivity in the $D^0 \to \overline{K}^0\pi^+\pi^-\pi^0$ final state is further reduced since we cannot tell if an individual candidate event arises from a D^0 decay or a $\overline{D}^0$ decay. Furthermore, the resonant substructure is potentially very complicated, with many decay modes contributing. However, using information from the other final states, it is possible to make useful measurements of the resonant substructure in this final state.

A. $D^0 \to K^-\pi^+\pi^+\pi^-$

The two-body decay modes which can contribute to the $K^-\pi^+\pi^+\pi^-$ final state include $K^-a_1(1260)^+$, $\overline{K}^{*0}\rho^0$, $K_1(1270)^-\pi^+$ and $K_1(1400)^-\pi^+$. Two three-body modes can also contribute: $\overline{K}^{*0}\pi^+\pi^-$ and $K^-\rho^0\pi^+$.

The results of the fit to this final state are shown in Table IV. Projections of the p.d.f. $\mathcal{F}$ onto events in the signal region are shown in Figure 2. The histograms, representing the projections of $\mathcal{F}$, are superimposed on data points. $\mathcal{F}_B$ is also drawn, scaled to the background level. Clear $\overline{K}^{*0}$ and ρ^0 peaks are visible and are well reproduced by the fit. A peak at the $K_1(1270)$ mass is visible in the $K^-(\pi^+\pi^-)_{\rm low}$ mass plot. The enhancement at low $K^-\pi^-$ mass, characteristic of the longitudinal polarization ($\lambda = 0$) of the $a_1(1260)$ in the $K^-a_1(1260)^+$ amplitude, is illustrated in Figure 3. The dip near 0.5 GeV/c^2 in the $(\pi^+\pi^-)_{\rm low}$ mass plot arises from the exclusion of $\pi^+\pi^-$ combinations which have a high probability of originating from a K_s decay.

The presence of the transverse $\overline{K}^{*0}\rho^0$ amplitude leads to distinctive angular correlations between $\overline{K}^{*0}$ and ρ^0 decays. We show an example in Figure 4. The transverse $\overline{K}^{*0}\rho^0$ amplitude is a sum of S-wave and D-wave amplitudes with destructive inter-

ference. At the bottom of Table IV, we show the results for $\overline{K}^{*0}\rho^0$ if partial wave amplitudes are used instead of helicity amplitudes.

In previous analyses [26–29], the resonant substructure of $D^0 \to K^-\pi^+\pi^+\pi^-$ decays was measured by fitting one-dimensional mass plots to obtain the $\overline{K}^{*0}\rho^0$, inclusive $\overline{K}^{*0}$, inclusive ρ^0, and nonresonant four-body branching fractions. In the present analysis, the likelihood function provides a complete description of the decay modes in the five-dimensional phase space. All the information available in the event is used in the fit, making it possible to use a general set of amplitudes, include interference, and obtain branching fractions for exclusive decay modes. A comparison with results from other experiments is shown in Table V. The inclusive $\bar{K}^*$ and ρ branching fractions are coherent sums of the appropriate exclusive fractions. Similarly, the coherent sum of all the two-body amplitudes is 76%.

B. $D^+ \to \overline{K}^0\pi^+\pi^+\pi^-$

The two-body decay modes which can contribute to the $\overline{K}^0\pi^+\pi^+\pi^-$ final state include $\overline{K}^0 a_1(1260)^+$, $\overline{K}_1(1270)^0\pi^+$ and $\overline{K}_1(1400)^0\pi^+$. No $\overline{K}^*\rho$ mode can contribute to this final state. There are two three-body modes which can contribute, $K^{*-}\pi^+\pi^+$ and $\overline{K}^0\rho^0\pi^+$.

The main features of the resonant substructure of this final state may be seen in the scatter plots in Figures 5(a) and 5(b). The notable features are a K^{*-} band, with clusters at high and low $(\pi^+\pi^-)_2$ mass, and a ρ^0 band, with clusters at high and low $\overline{K}^0\pi^-$ mass. In Figures 5(c) and 5(d), these features are reproduced with Monte Carlo events generated according to the results of the fit to the data, and include contributions from $\overline{K}^0 a_1(1260)^+$, $\overline{K}_1(1400)^0\pi^+$, and four-body nonresonant decays. These features are analogous to the enhancements at low $K^-\pi^-$ mass in $D^0 \to K^- a_1(1260)^+$ decays.

Although the $\overline{K}_1(1400)^0$ is very broad, with a width of 0.184 GeV, clustering of the K^{*-} band in the $\overline{K}_1(1400)^0$ regions is visible in the scatter plots in Figures 6(a) and 6(b). A cluster of K^{*-} events can also be seen extending into the low $\overline{K}^0(\pi^+\pi^-)_{\rm high}$ region, in contrast to events outside the K^{*-} band. This cluster, a kinematic reflection of the $\overline{K}_1(1400)^0$ in the $\overline{K}^0(\pi^+\pi^-)_{\rm low}$ plot, cannot be produced by any known amplitude other than the $\overline{K}_1(1400)^0\pi^+$ amplitude. Scatter plots of Monte Carlo data are shown in Figures 6(c) and 6(d).

Results of the fit are shown in Table VI. Projections of $\mathcal{F}$ onto events in the signal region are shown in Figure 7 for the $D^+ \to \overline{K}^0\pi^+\pi^+\pi^-$ final state. $\mathcal{F}_B$ is also drawn, scaled to the background level. The coherent sum of the two-body amplitudes is 83%.

C. $D^+ \to K^-\pi^+\pi^+\pi^0$

The two-body decay modes which can contribute to the $K^-\pi^+\pi^+\pi^0$ final state include $\overline{K}^{*0}\rho^+$, $\overline{K}_1(1270)^0\pi^+$ and $\overline{K}_1(1400)^0\pi^+$. No $\overline{K}a_1(1260)$ mode can contribute to this final state. There are three three-body modes which can contribute: $K^{*-}\pi^+\pi^+$, $\overline{K}^{*0}\pi^+\pi^0$ and $K^-\rho^+\pi^+$.

The results of the fit are shown in Table VII. Projections of $\mathcal{F}$ onto events in the signal region are shown in Figure 8. $\mathcal{F}_B$ is also drawn, scaled to the background level. Large $\overline{K}^{*0}$ peaks are seen in the $K^-\pi^+$ mass plot. Although there is a large peak in $K^-\pi^0$ mass, it is too high in mass to fit a K^{*-} Breit–Wigner propagator, and is assumed to be a fluctuation. The coherent sum of the two-body amplitudes is 82%.

The fraction of $\overline{K}_1(1400)^0\pi^+$ is 0.40 ± 0.10, in excellent agreement with the value expected from the results of the analysis of the $D^+ \to \overline{K}^0\pi^+\pi^+\pi^-$ final state. The fraction for $\overline{K}^{*0}\rho^+$ is very large, 0.56 ± 0.08. In contrast to the $K^-\pi^+\pi^+\pi^-$ final state, both transverse and longitudinal helicities yield significant contributions corresponding to the S-wave amplitude, in which case the Lorentz-invariant amplitude for the

total $\overline{K}^{*0}\rho^+$ assumes a very simple form when expressed in terms of three-momenta in the rest frame of the $\overline{K}^{*0}$:

$$A_{\overline{K}^{*0}\rho^+} = (\vec{p}_{K^-} - \vec{p}_{\pi_1^+}) \cdot (\vec{p}_{\pi^0} - \vec{p}_{\pi_2^+}) \quad , \tag{29}$$

where π_1^+ is the pion from the $\overline{K}^{*0}$. From this expression, we expect a distribution proportional to $\cos^2\theta_{VV}$, where θ_{VV} is the angle between the two three-vectors in the dot-product. Figure 9, a scatter plot of $K^-\pi_1^+$ mass vs. $\cos\theta_{VV}$, shows the expected behavior.

D. $D^0 \to \overline{K}^0\pi^+\pi^-\pi^0$

In this analysis, we cannot tell if an individual $\overline{K}^0\pi^+\pi^-\pi^0$ candidate event arises from a D^0 decay or a $\overline{D}^0$ decay. To deal with this problem, we form a total p.d.f. out of the p.d.f. for each hypothesis:

$$\mathcal{F}_S = \mathcal{F}_{D^0} + \mathcal{F}_{\overline{D}^0} \quad . \tag{30}$$

The limited statistical sample in this final state makes it necessary to adopt the following set of simplifying assumptions:

1. Several of the decay modes contributing to this final state have already been measured in the $K^-\pi^+\pi^+\pi^-$ final state. We constrain the relative fractions and phases of the amplitudes for $\overline{K}^{*0}\rho^0$ (transverse), $K_1(1270)^-\pi^+$, and $\overline{K}^{*0}\pi^+\pi^-$ to the values expected from these measurements. Isospin calculations are required to convert both the relative fractions *and* phases in one final state to those expected in another final state. The overall fraction of these amplitudes is allowed to vary, providing a consistency check. The relative fractions and phases are allowed to vary within errors.

2. When an amplitude for P-wave $K^{*-}\rho^+$ is included, the fraction can be as large as $20 \pm 7\%$. The stringent upper limits on P-wave $\overline{K}^{*0}\rho^0$ and $\overline{K}^{*0}\rho^+$ decays combined with the isospin relations rule out the possibility of a fraction for P-wave $K^{*-}\rho^+$ above 9%. Therefore, we leave this amplitude out of the final fit. However, the variations in the other fractions when this amplitude is included in the fit are included in the systematic errors.

3. When amplitudes for $\overline{K}_1(1270)^0\pi^0$ are included, the fraction is as large as $18 \pm 9\%$. Given the measurement of $K_1(1270)^-\pi^+$, the upper limit on $\overline{K}_1(1270)^0\pi^+$, and the isospin relations, we can calculate a maximum plausible value for $\overline{K}_1(1270)^0\pi^0$. We estimate a 90% C.L. upper limit of 3.2% for $K_1(1270)^-\pi^+$, and use the previously derived upper limit of 1.1% for $\overline{K}_1(1270)^0\pi^+$. We assume a relative phase of π between $A_{1/2}$ and $A_{3/2}$ so that the interference is maximally destructive for $K_1(1270)^-\pi^+$ and constructive for $\overline{K}_1(1270)^0\pi^0$. We find that the fraction for $\overline{K}_1(1270)^0\pi^0$ cannot be more than 10%. As we are not sensitive to a fraction this large, we leave the amplitudes for $\overline{K}_1(1270)^0\pi^0$ out of the fits. However, the variations in the fractions as this amplitude is included in the fit is included in the systematic errors.

4. There are five different types of three-body amplitudes which can contribute to this final state, $\overline{K}^0\rho^0\pi^0$, $\overline{K}^0\rho^-\pi^+$, $\overline{K}^0\rho^+\pi^-$, $\overline{K}^{*0}\pi^+\pi^-$, and $K^{*-}\pi^+\pi^0$. Each of these comes in six different partial waves, assuming there is only one unit of angular momentum. None of these amplitudes are statistically significant. We include them one at a time, to obtain the systematic errors on the other fractions.

The results of the fit are shown in Table VIII. Projections of $\mathcal{F}$ onto events in the signal region are shown in Figure 10. $\mathcal{F}_B$ is also drawn, scaled to the background level.

There is a $\overline{K}^*$ peak visible in the $(\overline{K}^0\pi^\mp)_1$ mass plot and a strong ω peak visible in the $\pi^+\pi^-\pi^0$ mass plot. There is no enhancement evident at low $\overline{K}^0\pi^0$ mass, indicating that the $D^0 \to \overline{K}^0 a_1(1260)^0$ amplitude is small. The coherent sum of the two-body amplitudes is 79%.

For the ω line-shape, a Breit–Wigner function is convoluted with a Gaussian resolution function [30]. The resolution predicted by the Monte Carlo is 0.0087 GeV/c^2. Interference between the $\overline{K}^0\omega$ amplitude and other amplitudes is ignored. To obtain the $\overline{K}^0\omega$ amplitude, we evaluate the following triple product, where the three-momenta are evaluated in the ω frame:

$$A_{\overline{K}^0\omega} = \vec{p}_K \cdot (\vec{p}_{\pi^+} \times \vec{p}_{\pi^-}) \quad . \tag{31}$$

We have also obtained several upper limits from the analysis of these four final states. These are shown in Table IX.

V. ISOSPIN DECOMPOSITIONS

We combine results from the analysis of the four final states. Using these results, we perform an isospin decomposition on several two-body decay modes.

A. $D \to \overline{K} a_1(1260)$

We have obtained measurements of the branching fractions for $K^- a_1(1260)^+$ and $\overline{K}^0 a_1(1260)^+$ and a stringent upper limit on that for $\overline{K}^0 a_1(1260)^0$. The latter is expected to be zero in the BSW model. However, the large branching fractions for the first two decay modes could have made the branching fraction for $\overline{K}^0 a_1(1260)^0$ large through final state interactions. The upper limit, therefore, is very useful for placing limits on the effects of final state interactions, thereby eliminating this source of ambiguity in the comparison of measurements with models.

We list the measurements, predictions, and isospin decomposition for $\overline{K}a_1(1260)$ in Table X. We define $\delta \equiv \delta_{1/2} - \delta_{3/2}$. The central values for the branching fractions of the three $\overline{K}a_1(1260)$ modes are close to the edge of the space allowed by the isospin relations. We therefore perform a fit in which we vary the three branching fractions within their errors, but apply the constraint of the isospin relations, in order to obtain new values and errors for the branching fractions, and values and errors for δ and $|A_{1/2}/A_{3/2}|$. We use $B(D^0 \to \overline{K}^0 a_1(1260)^0) = (0.4 \pm 0.4 \pm 0.9)\%$ for this fit. The ratio of isospin amplitudes is $2.8 \pm 0.4 \pm 0.3$, consistent with that found in PP and PV decays. The measured branching fractions are much higher than the BSW predictions.

B. $D \to \overline{K}^* \rho$

We have obtained measurements of the branching fractions to the three $\overline{K}^* \rho$ modes. BSW have made predictions for each of these modes. We list the measurements and predictions, along with the isospin decomposition, in Table XI, as well as the BSW predictions, recalculated with the measured value of the isospin phase shift. Again, the ratio of isospin amplitudes is in the range found for PP and PV modes.

The branching fraction for $\overline{K}^{*0}\rho^0$ was first reported in Reference 31, and was found to be in good agreement with the value predicted by BSW. Now that the branching fractions for the other two $\overline{K}^* \rho$ modes have been measured, and isospin phase shifts have been taken into account, we find that the branching fractions for $\overline{K}^* \rho$ are much smaller than the predicted values.

We find that in the $\overline{K}^{*0}\rho^0$ mode, the $\overline{K}^{*0}$ and ρ^0 are completely transversely polarized ($\lambda = \pm 1$), requiring a mixture of S- and D-wave amplitudes such that the longitudinal components of these two amplitudes cancel. We have placed an upper limit on the P-wave component. For the $\overline{K}^{*0}\rho^+$ mode, we find a mixture of

transverse and longitudinal polarization consistent with a pure S-wave amplitude. We have placed limits on the P- and D-wave components. For the $K^{*-}\rho^+$ mode, we are not sensitive to the polarization. A limit on P-wave $K^{*-}\rho^+$ is obtained using the other two $\overline{K}^*\rho$ modes and the isospin relations, and is shown in Table IX.

C. $D \to \overline{K}_1(1270)\pi$

We have obtained a measurement of the branching fraction to $K_1(1270)^-\pi^+$, and an upper limit on that to $\overline{K}_1(1270)^0\pi^+$. We can place a lower limit on the ratio of isospin amplitudes in this mode. Using a conservative lower bound of 0.73% on the branching fraction to $K_1(1270)^-\pi^+$ and combining this with the upper limit on that to $\overline{K}_1(1270)^0\pi^+$, assuming maximum constructive interference between the isospin amplitudes for $K_1(1270)^-\pi^+$, we obtain a conservative lower limit on the ratio of isospin amplitudes. The results are summarized in Table XII. The limit on $\overline{K}_1(1270)^0\pi^0$ is derived from the results for the other two $\overline{K}_1(1270)\pi$ modes and the isospin relations.

D. $D \to \overline{K}_1(1400)\pi$

We have obtained a measurement of the branching fraction to $\overline{K}_1(1400)^0\pi^+$, and upper limits on those to $K_1(1400)^-\pi^+$ and $\overline{K}_1(1400)^0\pi^0$. We estimate a 90% C.L. lower limit of 1.9% for $\overline{K}_1(1400)^0\pi^+$. Combining this with the two upper limits, we obtain the largest plausible value of the ratio of isospin amplitudes. The results are summarized in Table XIII.

E. Summary of Isospin Decompositions

In Table XIV we gather the results on the isospin decompositions from this paper, together with the results from Reference 6. As discussed in Section I, the ratios of isospin amplitudes for the PP and PV modes correspond to the lifetime ratio of the

D^0 and D^+. For the VV and PA decays $\overline{K}^*\rho$ and $\overline{K}a_1(1260)$, we find the ratios of isospin amplitudes to be $2.8\pm0.4\pm0.3$ and $3.4\pm0.7\pm0.7$. These values also correspond to the lifetime difference of the D mesons, and confirm that an understanding of this difference requires an understanding of two-body decay modes.

VI. FORM FACTORS

In models of semileptonic charm decay, the matrix element in Equation (7) is typically parametrized in terms of a Lorentz invariant matrix element multiplied by a form factor. The Lorentz invariant matrix element contains the dependence on the spins and four-momenta of the particles involved. The form factor contains the dependance on q^2, where q^μ is the four-momentum of the $\bar{\ell}\nu$ system, or of the meson m in the hadronic case. The form factors are typically calculated at one value of q^2, and extrapolated to other values of q^2 using a single pole function. Under the assumption of factorization, the decays $D^0 \rightarrow K^{*-}\rho^+$ and $D^+ \rightarrow \overline{K}^{*0}e^+\nu$ both depend on the same $D \rightarrow \overline{K}^*$ form factors.

The E691 Collaboration has measured the branching fraction for $D^+ \rightarrow \overline{K}^{*0}e^+\nu$ to be $(4.5 \pm 0.7 \pm 0.5)\%$ [15]. This value is lower than the Mark III result $(7.7 \pm 1.3)\%$ obtained from a global fit to several exclusive semileptonic branching fractions, inclusive semileptonic branching fractions, and the charmed meson lifetimes [9]. The E691 measurements of the form factors for this decay indicate that the form factors are not predicted correctly by the models, as shown in Table XV. Mark III has obtained a result for the ratio of longitudinal to transverse polarization of the $\overline{K}^{*0}$, Γ_L/Γ_T, but not for the individual form factors.

While the decay $D^0 \rightarrow K^{*-}\rho^+$ depends on $D \rightarrow \overline{K}^*$ form factors, the decay $D^0 \rightarrow \overline{K}^{*0}\rho^0$ depends on $D \rightarrow \rho$ form factors, and the decay $D^+ \rightarrow \overline{K}^{*0}\rho^+$ depends on both $D \rightarrow \overline{K}^*$ and $D \rightarrow \rho$ form factors. The values of these form factors as

calculated in the BSW model are shown in Table XVI. These values are used for the predictions in Table XI. If we substitute the E691 form factors into the BSW model, we obtain the results in the column labeled "BSW 1" in Table XVII. We have assumed that the $D \to \rho$ form factors are equal to the $D \to \overline{K}^*$ form factors. These results are much closer to the measured values than the predictions in Table XI. Thus, the disagreement of the predictions from the data may be due to problems with the form factor predictions rather than with the factorization hypothesis. In the column labeled "BSW 2" in Table XVII, we have listed the predictions of the BSW model using the E691 form factors scaled by the square root of the Mark III $D^+ \to \overline{K}^{*0} e^+ \nu$ branching fraction. This scaling somewhat worsens the agreement with the model, but is still better than the original prediction.

We can gain additional information on these form factors from our studies of $D \to \overline{K}^* \rho$. While we do not have enough information on polarization in $D^0 \to K^{*-}\rho^+$, and the mode $D^0 \to \overline{K}^{*0}\rho^0$ is strongly affected by isospin phase shifts, the decay $D^+ \to \overline{K}^{*0}\rho^+$ is theoretically relatively simple. Weak annihilation is possible only for D^0 decays. This mode is unaffected by isospin phase shifts, and inelastic final state interactions should be small because they must proceed through the exotic $I = 3/2$ channel. A disadvantage of the analysis of this decay mode is that it involves a subtraction of two terms, the first proportional to the $D \to \overline{K}^*$ form factors, and the second the $D \to \rho$ form factors.

The matrix element for the decay $D \to V_1 V_2$ has three terms. The first is an S-wave term, proportional to the form factor $A_1(q^2)$:

$$\varepsilon_1 \cdot \varepsilon_2 \quad , \tag{32}$$

where ε_1 and ε_2 are the polarization vectors of V_1 and V_2. The second is a P-wave term, proportional to the form factor $V(q^2)$:

$$\epsilon_{\alpha\beta\gamma\delta} P^\alpha Q^\beta \varepsilon_1^\gamma \varepsilon_2^\delta \quad , \tag{33}$$

where P^μ is the sum of the four-momenta of V_1 and V_2 and Q^μ is the difference. The third is the longitudinal component of a D-wave term, proportional to the form factor $A_2(q^2)$:

$$(\varepsilon_1 \cdot Q)(\varepsilon_2 \cdot Q) \quad . \tag{34}$$

The predictions of the BSW model for $\overline{K}^* \rho$ for these three terms are shown in Table XVIII. We see that in the BSW model, the S-wave term is dominant, in agreement with our observation in $D^+ \to \overline{K}^{*0} \rho^+$ decays. However, it is notable that in the decay mode $\overline{K}^{*0} \rho^0$, the $\overline{K}^{*0}$ and ρ^0 are transversely polarized ($\lambda = \pm 1$). Thus the amplitude for this decay mode is a combination of S- and D-wave states. A large D-wave contribution would not be consistent with the factorization hypothesis.

In our study of polarization in $D^+ \to \overline{K}^{*0} \rho^+$ decays, we have found that the data is well described by an S-wave amplitude as in Equation (32). We have set limits on P-wave and longitudinal D-wave amplitudes. If S-wave and D-wave terms are included in the fit, the fractions become $(71.6 \pm 10)\%$ and $(2.4 \pm 2.9)\%$ respectively, with an interference term of -18.5% so the total remains 55.5%. This is approximately what is expected in the BSW model: A small D-wave term and a larger interference term. We therefore use $(71.6 \pm 10 \pm 11)\%$ for the S-wave fraction when placing constraints on the A_1 form factors.

Assuming factorization, we can now place the following constraints on the form factors:

$$\begin{aligned} |7.18 a_1 A_1(0)_{D \to \overline{K}^*} + 8.38 a_2 A_1(0)_{D \to \rho}| &= 2.4 \pm 0.5 \quad , \\ |1.06 a_1 V(0)_{D \to \overline{K}^*} + 1.40 a_2 V(0)_{D \to \rho}| &< 0.7 \quad , \\ |0.84 a_1 A_2(0)_{D \to \overline{K}^*} + 1.05 a_2 A_2(0)_{D \to \rho}| &< 0.8 \quad , \end{aligned} \tag{35}$$

where a_1 and a_2 are the parameters of the BSW model. Using $a_1 = 1.2$ and $a_2 = -0.5$ and the E691 values for the $D \to \overline{K}^*$ form factors, we may solve for the $D \to \rho$ form factors. Since we take the absolute value of the left side of Equation (35), there are two solutions. For the $A_1(0)_{D\to\rho}$ form factor, we list both solutions. For the other form factors, we quote the more conservative upper limit:

$$\begin{aligned} A_1(0)_{D\to\rho} &= 0.4 \pm 0.2 \text{ (solution 1)} \quad , \\ &= 1.5 \pm 0.2 \text{ (solution 2)} \quad , \\ V(0)_{D\to\rho} &< 3.4 \quad , \\ A_2(0)_{D\to\rho} &< 2.2 \quad . \end{aligned} \tag{36}$$

VII. CONCLUSIONS

We have measured the resonant substructure of four $D \to \overline{K}\pi\pi\pi$ final states. We have found that these final states are dominated by two new types of two-body decay modes, VV and PA. We have measured branching fractions for the $\overline{K}a_1(1260)$, $\overline{K}^*\rho$, $\overline{K}_1(1270)\pi$, $\overline{K}_1(1400)\pi$, and $\overline{K}^0\omega$ decay modes. For the $\overline{K}a_1(1260)$ and $\overline{K}^*\rho$ decay modes, we have measured branching fractions for all three isospin combinations. This has allowed us to determine the effects of isospin phase shifts on the branching fractions, allowing an improved comparison of the data with the model of Bauer, Stech, and Wirbel. The branching fractions for the $\overline{K}a_1(1260)$ modes are much larger than the predictions, while the branching fractions for the $\overline{K}^*\rho$ decay modes are a factor of three smaller than predicted.

We have doubled the number of measured branching fractions for Cabibbo-allowed D^+ decays. We have extended, from 38% to 62% for the D^0, and 33% to 60% for the D^+, the fraction of the hadronic widths of the D mesons accounted for by two-body decays. It was shown in Section I that the widths for PP and PV decay modes of the D^0 and D^+ are proportional to the total hadronic widths of the D^0 and D^+. We

find this is also true for $\overline{K}a_1(1260)$ and $\overline{K}^*\rho$ decays. Thus, we confirm the hypothesis that an understanding of the lifetime ratio of the charmed mesons depends on an understanding of their two-body decays.

We have obtained detailed information on the helicity distributions in $\overline{K}^*\rho$ decays. In agreement with the BSW model, we find that the S-wave term is dominant for $D^+ \to \overline{K}^{*0}\rho^+$ decays. However, for $D^0 \to \overline{K}^{*0}\rho^0$ decays, we find a significant D-wave component, in contradiction with the factorization predictions. However, in D^0 decays, there may be large effects from final state interactions and weak annihilation. Assuming factorization, we have placed constraints on the $D \to \overline{K}^*$ and $D \to \rho$ form factors, as shown in Equation (35). These constraints may be used to test the factorization hypothesis, as the same form factors are measured in semileptonic D decays.

A recent analysis by the E691 collaboration has measured the $D \to \overline{K}^*$ form factors in the decay $D^+ \to \overline{K}^{*0}e^+\nu$. The results are not in agreement with theoretical models. If the factorization hypothesis is valid, these form factors should also apply to $D^0 \to K^{*-}\rho^+$ decays. The BSW predictions for $\overline{K}^*\rho$ decays are three times larger than the branching fractions measured in the present analysis. If we substitute the form factors measured by E691 into the BSW model and assume that the $D \to \overline{K}^*$ and $D \to \rho$ form factors are equal, we obtain good agreement with our measured values. If we substitute E691 form factors scaled to the Mark III $D^+ \to \overline{K}^{*0}e^+\nu$ branching fraction, the agreement is not as good. Future measurements of $D \to \overline{K}^*\ell\nu_\ell$ and $D \to \rho\ell\nu_\ell$ will enable a more precise test of factorization [32].

ACKNOWLEDGEMENTS

We gratefully acknowledge the dedicated efforts of the SPEAR staff. One of us (G.E.) wishes to thank the Heisenberg Foundation for support. This work was supported by the Department of Energy under contracts DE-AC03-76SF00515, DE-AC02-76ER01195, DE-AC03-81ER40050, DE-AC02-87ER40318, and DE-AM03-76SF00010; and also by the National Science Foundation.

REFERENCES

1. D. G. Hitlin, in *Int. Symp. on Lepton and Photon Interactions at High Energies, Hamburg, 1987,* edited by W. Bartel and R. Rückl (North-Holland, 1988).

2. P. E. Karchin, in *Int. Symp. on Lepton and Photon Interactions at High Energies, Stanford, 1989,* edited by M. Riordan (World Scientific, 1990).

3. We adopt the convention that "n-body decay mode" refers to a decay to n states which may be either long-lived particles or intermediate resonances, while "n-particle final state" refers to having n long-lived particles in the final state after the decay of the intermediate resonances.

4. R. H. Schindler *et al., Phys. Rev.* **D24**, 78 (1981).

5. D. J. Summers *et al., Phys. Rev. Lett.* **52**, 410 (1984).

6. J. Adler *et al., Phys. Lett.* **196B**, 107 (1987).

7. J. C. Anjos *et al., Phys. Rev. Lett.* **60**, 897 (1988).

8. J. J. Hernandez *et al.* (Particle Data Group), *Phys. Lett.* **239B**, 1 (1990).

9. Z. Bai *et al., Phys. Rev. Lett.* **66**, 1011 (1991).

10. We adopt the convention that reference to a state implies reference to its charge conjugate.

11. Further details may be found in: D. F. DeJongh, Ph.D. thesis, California Institute of Technology, 1990.

12. M. Bauer, B. Stech, and M. Wirbel, *Z. Phys.* **C34**, 103 (1987). Revised values of $a_1 = 1.2$ and $a_2 = -0.5$ are taken from B. Stech, preprint HD-THEP-87-18, 1987 (unpublished).

13. A. N. Kamal and R. C. Verma, preprint Alberta-Thy-5-91A.

14. The predictions for $\overline{K}a_1(1260)$ in Reference 12 assume a narrow $a_1(1260)$. There was a private communication from B. Stech which indicated that including the $a_1(1260)$ width changed the prediction considerably. A detailed calculation by Kamal and Verma [13] does not substantiate this.

15. J. C. Anjos *et al., Phys. Rev. Lett.* **65**, 2630, (1990).

16. J. Hauser, Ph.D. thesis, California Institute of Technology, 1985.

17. R. M. Baltrusaitis *et al., Phys. Rev. Lett.* **56**, 2140 (1986).

18. J. Adler *et al., Phys. Rev. Lett.* **60**, 89 (1988).

19. D. Bernstein *et al., Nucl. Instrum. Methods* **226**, 301 (1984).

20. J. C. Anjos *et al., Phys. Lett.* **223B**, 267 (1989).

21. H. M. Pilkuhn, *Relativistic Particle Physics* (Springer-Verlag, New York, 1979). p. 174.

22. J. D. Richman, Ph.D. thesis, California Institute of Technology, 1985.

23. J. C. Anjos *et al., Phys. Rev. Lett.* **62**, 722 (1989).

24. J. D. Jackson, *Nuovo Cimento,* Vol. XXXIV, N. 6, 1645 (1964).

25. M. G. Bowler, *Phys. Lett.* **209B**, 99 (1988).

26. M. Piccolo *et al., Phys. Lett.* **70B**, 260 (1977).

27. R. Bailey *et al., Phys. Lett.* **132B**, 237 (1983).

28. P. Kim, Ph.D. thesis, University of Toronto, 1987.

29. J. C. Anjos *et al.,* contributed paper, International Conference on Energy Physics, Munich, 1988.

30. W. S. Lockman, Santa Cruz Institute for Particle Physics preprint SCIPP 89/08, p. 59.

31. J. Adler *et al., Phys. Rev. Lett.* **64**, 2615 (1990).

32. We anticipate results from Fermilab experiments E653, E687, and E791.

33. B. Grinstein *et al., Phys. Rev.* **D39**, 799 (1989).

34. M. Bauer, B. Stech, and M. Wirbel, *Z. Phys.* **C29**, 637 (1985).

35. F. J. Gilman and R. L. Singleton, *Phys. Rev.* **D41**, 142 (1990).

36. J. G. Korner and G. A. Schuler, *Z. Phys.* **C38**, 511 (1988); *ibid.*, **41**, 690(E) (1989).

TABLE I. Relative branching fractions of various two-body decay modes to four-particle final states. In addition to the four final states we study, there are three additional final states, which have too many neutral particles to detect efficiently.

	$D^0 \to$				$D^+ \to$		
Mode	$K^-\pi^+\pi^+\pi^-$	$\overline{K}^0\pi^+\pi^-\pi^0$	$K^-\pi^+\pi^0\pi^0$	$\overline{K}^0\pi^0\pi^0\pi^0$	$\overline{K}^0\pi^+\pi^+\pi^-$	$K^-\pi^+\pi^+\pi^0$	$\overline{K}^0\pi^+\pi^0\pi^0$
$\overline{K}^0 a_1(1260)^+$					1/2		1/2
$K^- a_1(1260)^+$	1/2		1/2				
$\overline{K}^0 a_1(1260)^0$		1					
$\overline{K}^{*0}\rho^+$						2/3	1/3
$K^{*-}\rho^+$		2/3	1/3				
$\overline{K}^{*0}\rho^0$	2/3	1/3					
$\overline{K}_1(1270)^0\pi^+$					0.34	0.48	0.05
$K_1(1270)^-\pi^+$	0.34	0.48	0.05				
$\overline{K}_1(1270)^0\pi^0$		0.34	0.48	0.05			
$\overline{K}_1(1400)^0\pi^+$					4/9	4/9	1/9
$K_1(1400)^-\pi^+$	4/9	4/9	1/9				
$\overline{K}_1(1400)^0\pi^0$		4/9	4/9	1/9			
Number of events	1281	140			209	142	
Backgrounds	Low	High			Low	Medium	

TABLE II. Lorentz invariant amplitudes. Given a vertex $A \to B+C$, A, B, and C have 4-momenta p_A, p_B, and p_C respectively; $q_A = p_B - p_C$ is the difference between the outgoing momenta. Pseudo-scalar, scalar, vector, axial vector and tensor states are denoted by P, S, V, A, and T respectively.

Mode	Amplitude
$D \to PP_1$, $P \to VP_2$, $V \to P_3P_4$	$p^\mu_{P_2}(g^{\mu\nu} - p^\mu_V p^\nu_V / M^2_V) q^\nu_V$
$D \to AP_1$, $A \to VP_2$ $V \to P_3P_4$	$p^\mu_{P_1}(g^{\mu\nu} - p^\mu_A p^\nu_A / M^2_A)(g^{\nu\sigma} - p^\nu_V p^\sigma_V / M^2_V) q^\sigma_V$
$D \to AP_1$, $A \to SP_2$, $S \to P_3P_4$	$p^\mu_{P_1}(g^{\mu\nu} - p^\mu_A p^\nu_A / M^2_A) q^\nu_A$
$D \to V_1V_2$, $V_1 \to P_1P_2$, $V_2 \to P_3P_4$ (V_1 and V_2 in relative S-wave.)	$q^\mu_{V_1}(g^{\mu\nu} - p^\mu_{V_1} p^\nu_{V_1} / M^2_{V_1})(g^{\nu\sigma} - p^\nu_{V_2} p^\sigma_{V_2} / M^2_{V_2}) q^\sigma_{V_2}$
$D \to V_1V_2$, $V_1 \to P_1P_2$, $V_2 \to P_3P_4$ (V_1 and V_2 in relative P-wave.)	$\epsilon_{\alpha\beta\gamma\delta} p^\alpha_D q^\beta_D q^\gamma_{V_1} q^\delta_{V_2}$
$D \to V_1V_2$, $V_1 \to P_1P_2$, $V_2 \to P_3P_4$ (Longitudinal D-wave.)	$q^\mu_{V_1}(g^{\mu\nu} - p^\mu_{V_1} p^\nu_{V_1} / M^2_{V_1}) p^\nu_{V_2}$ $\times\, q^\mu_{V_2}(g^{\mu\nu} - p^\mu_{V_2} p^\nu_{V_2} / M^2_{V_2}) p^\nu_{V_1}$
$D \to VS$, $V \to P_1P_2$, $S \to P_3P_4$	$p^\mu_S(g^{\mu\nu} - p^\mu_V p^\nu_V / M^2_V) q^\nu_V$
$D \to V_1P_1$, $V_1 \to V_2P_2$, $V_2 \to P_3P_4$	$\epsilon_{\alpha\beta\gamma\delta} p^\alpha_{V_1} q^\beta_{V_1} p^\gamma_{P_1} q^\delta_{V_2}$
$D \to TP_1$, $T \to VP_2$, $V \to P_3P_4$	$((p_{P_1} \cdot q_T) - (p_{P_1} \cdot p_T)(q_T \cdot p_T)/M^2_T)$ $\times\, \epsilon_{\alpha\beta\gamma\delta} p^\alpha_T q^\beta_T q^\gamma_V p^\delta_{P_1}$
Three-body nonresonant	Substitute $1/p^2$ for $1/M^2$.
Four-body nonresonant	Constant

TABLE III. Decay chains. The subscript "A" denotes an axial vector state, while the subscript "P" denotes a pseudoscalar state. The relative fractions of the three decay modes of the $\overline{K}_1(1270)$ are constrained within errors to those of the Particle Data Group [8] multiplied by the appropriate Clebsch-Gordon coefficients. The relative phases are allowed to vary.

$D^0 \to K^- a_1(1260)^+$	$a_1(1260)^+ \to \rho^0\pi^+$	$\rho^0 \to \pi^-\pi^+$
$D^0 \to K^{*-}\rho^+$	$K^{*-} \to \overline{K}^0\pi^-$	$\rho^+ \to \pi^+\pi^0$
$D^0 \to \overline{K}^{*0}\rho^0$	$\overline{K}^{*0} \to K^-\pi^+$	$\rho^0 \to \pi^+\pi^-$
$D^0 \to K_1(1270)^-\pi^+$		
$K_1(1270)^- \to$	$\rho^0 K^-$	$\rho^0 \to \pi^+\pi^-$
	$\overline{K}_0^*(1430)^0\pi^-$	$\overline{K}_0^{*0} \to K^-\pi^+$
	$\overline{K}^{*0}\pi^+$	$\overline{K}^{*0} \to K^-\pi^+$
$D^0 \to (\overline{K}^{*0}\pi^-)_P\pi^+$	$(\overline{K}^{*0}\pi^-)_P \to \overline{K}^{*0}\pi^-$	$\overline{K}^{*0} \to K^-\pi^+$
$D^0 \to (\rho^0 K^-)_A\pi^+$	$(\rho^0 K^-)_A \to \rho^0 K^-$	$\rho^0 \to \pi^+\pi^-$
$D^+ \to \overline{K}^0 a_1(1260)^+$	$a_1(1260)^+ \to \rho^0\pi^+$	$\rho^0 \to \pi^-\pi^+$
$D^+ \to \overline{K}^{*0}\rho^+$	$\overline{K}^{*0} \to K^-\pi^+$	$\rho^+ \to \pi^+\pi^0$
$D^+ \to \overline{K}_1(1400)^0\pi^+$	$\overline{K}_1(1400)^0 \to K^{*-}\pi^+$	$K^{*-} \to \overline{K}^0\pi^-$
$D^+ \to \overline{K}_1(1400)^0\pi^+$		
$\overline{K}_1(1400)^0 \to$	$\overline{K}^{*0}\pi^0$	$\overline{K}^{*0} \to K^-\pi^+$
	$K^{*-}\pi^+$	$K^{*-} \to K^-\pi^0$
$D^+ \to (\rho^+ K^-)_A\pi^+$	$(\rho^+ K^-)_A \to \rho^+ K^-$	$\rho^+ \to \pi^+\pi^0$

TABLE IV. Results for $D^0 \to K^-\pi^+\pi^+\pi^-$. At the bottom, we show the results for $\overline{K}^{*0}\rho^0$ if partial wave amplitudes are used instead of helicity amplitudes.

Amplitude	Relative Fraction f_i	Phase α_i	Branching Fraction (%)
Four-body nonresonant	$0.242 \pm 0.025 \pm 0.06$	-1.07 ± 0.08	$2.2 \pm 0.3 \pm 0.6$
$\overline{K}^{*0}\rho^0$ transverse	$0.142 \pm 0.016 \pm 0.05$	1.75 ± 0.09	$1.9 \pm 0.3 \pm 0.7$
$K^-a_1(1260)^+$	$0.492 \pm 0.024 \pm 0.08$	0	$9.0 \pm 0.9 \pm 1.7$
$K_1(1270)^-\pi^+$	$0.066 \pm 0.019 \pm 0.03$	0.71 ± 0.25	$1.8 \pm 0.5 \pm 0.8$
$\overline{K}^{*0}\pi^+\pi^-$	$0.140 \pm 0.018 \pm 0.04$	3.07 ± 0.09	$1.9 \pm 0.3 \pm 0.6$
$K^-\rho^0\pi^+$	$0.084 \pm 0.022 \pm 0.04$	-0.30 ± 0.13	$0.8 \pm 0.2 \pm 0.4$
$\overline{K}^{*0}\rho^0$ S-wave	$0.327 \pm 0.046 \pm 0.05$	1.69 ± 0.10	$4.5 \pm 0.7 \pm 0.8$
$\overline{K}^{*0}\rho^0$ D-wave longitudinal	$0.161 \pm 0.027 \pm 0.05$	1.96 ± 0.12	$2.2 \pm 0.4 \pm 0.7$

TABLE V. Fractions of the $K^-\pi^+\pi^+\pi^-$ final state as observed by different experiments.

Channel	Mark III	SLAC–LBL[a]	ACCMOR[b]	ARGUS[c]	E691[d]
$\overline{K}^{*0}$ + X	$0.207 \pm 0.020 \pm 0.03$			0.39 ± 0.03	$0.26 \pm 0.04 \pm 0.03$
ρ^0 + X	$0.855 \pm 0.032 \pm 0.03$			0.86 ± 0.10	$1.06 \pm 0.06 \pm 0.09$
$\overline{K}^{*0}\rho^0$	$0.142 \pm 0.016 \pm 0.05$	$0.1^{+0.11}_{-0.10}$	0.5 ± 0.2	0.35 ± 0.06	
$K^-\rho^0\pi^+$	$0.084 \pm 0.022 \pm 0.04$	$0.85^{+0.11}_{-0.22}$	0.2 ± 0.2	0.51 ± 0.08	
$K^-a_1(1260)^+$	$0.492 \pm 0.024 \pm 0.08$			0.51 ± 0.08[e]	
$\overline{K}^{*0}\pi^+\pi^-$	$0.140 \pm 0.018 \pm 0.04$	$0.0^{+0.2}_{-0.0}$	< 0.18	0.04 ± 0.04	
$K^-\pi^+\pi^+\pi^-$	$0.242 \pm 0.025 \pm 0.06$	$0.05^{+0.11}_{-0.05}$		0.11 ± 0.06	

[a] Reference 26.

[b] Reference 27.

[c] Reference 28.

[d] Reference 29.

[e] In the ARGUS analysis, angular distributions of ρ^0 decays outside the $\overline{K}^{*0}$ bands were examined. The $K^-\rho^0\pi^+$ component was found to be consistent with being entirely $K^-a_1(1260)^+$.

TABLE VI. Results for $D^+ \to \overline{K}^0\pi^+\pi^+\pi^-$.

Amplitude	Fraction (%)	Phase	Branching Fraction (%)
Four-body nonresonant	$17.0 \pm 5.6 \pm 10.0$	1.09 ± 0.28	$1.1 \pm 0.4 \pm 0.7$
$\overline{K}^0 a_1(1260)^+$	$53.9 \pm 5.7 \pm 7.0$	0	$7.1 \pm 1.8 \pm 1.1$
$\overline{K}_1(1400)^0\pi^+$	$27.7 \pm 4.7 \pm 8.0$	-0.07 ± 0.32	$4.1 \pm 1.2 \pm 1.2$

TABLE VII. Results for $D^+ \to K^-\pi^+\pi^+\pi^0$.

Amplitude	Fraction (%)	Phase	Branching Fraction (%)
Four-body nonresonant	$18.4 \pm 7.0 \pm 5.0$	4.0 ± 0.22	$1.1 \pm 0.5 \pm 0.4$
$\overline{K}^{*0}\rho^+$ S-wave	$55.5 \pm 7.7 \pm 11.0$	0	$4.8 \pm 1.2 \pm 1.4$
$\overline{K}_1(1400)^0\pi^+$	$40.3 \pm 9.7 \pm 8.0$	3.4 ± 0.15	$5.3 \pm 1.7 \pm 1.5$
$K^-\rho^+\pi^+$	$15.9 \pm 6.5 \pm 6.0$	3.8 ± 0.25	$0.9 \pm 0.4 \pm 0.4$

TABLE VIII. Results for $D^0 \to \overline{K}^0\pi^+\pi^-\pi^0$.

Amplitude	Fraction (%)	Phase	Branching Fraction (%)
Four-body nonresonant	$21.0 \pm 14.7 \pm 15.0$	-0.45 ± 0.55	$2.2 \pm 1.6 \pm 1.7$
$K^{*-}\rho^+$ longitudinal	19.3 ± 7.4	0	
$K^{*-}\rho^+$ transverse	21.1 ± 12.0	2.0 ± 0.48	
$K^{*-}\rho^+$ total	$40.4 \pm 12.5 \pm 8.4$		$6.2 \pm 2.3 \pm 2.0$
$\overline{K}^0\omega$	$19.5 \pm 4.3 \pm 1.4$		$2.3 \pm 0.7 \pm 0.6$
$\overline{K}^{*0}\rho^0$ transverse	4.2 ± 3.7		1.3 ± 1.2
$K_1(1270)^-\pi^+$	4.8 ± 1.5		1.0 ± 0.4
$\overline{K}^{*0}\pi^+\pi^-$	12.7 ± 7.0		3.9 ± 2.3

TABLE IX. The 90% C.L. upper Limits from the four final states.

Amplitude	Branching Fraction (%)
$D^0 \to \overline{K}^{*0}\rho^0$ Longitudinal (S-wave)	< 0.3
$D^+ \to \overline{K}^{*0}\rho^+$ P-wave	< 0.5
$D^0 \to K^{*-}\rho^+$ P-wave	$< 1.5^a$
$D^0 \to \overline{K}^{*0}\rho^0$ P-wave	< 0.3
$D^+ \to \overline{K}^{*0}\rho^+$ Longitudinal D-wave	< 0.7
$D^+ \to \overline{K}_1(1270)^0\pi^+$	< 1.1
$D^0 \to K_1(1400)^-\pi^+$	< 1.2
$D^0 \to \overline{K}_1(1400)^0\pi^0$	< 3.7
$D^0 \to \overline{K}^0 a_1(1260)^0$	< 1.9
$D^0 \to K^- a_2(1320)^+$	< 0.6
$D^+ \to \overline{K}^0 a_2(1320)^+$	< 0.8
$D^0 \to K^*(1415)^-\pi^+$	< 1.2
$D^+ \to \overline{K}^*(1415)^0\pi^+$	< 0.7
$D^+ \to K^{*-}\pi^+\pi^+$	< 1.3
$D^+ \to \overline{K}^{*0}\pi^+\pi^0$	< 0.8
$D^+ \to \overline{K}^0\rho^0\pi^+$	< 0.4

[a] Obtained using other $\overline{K}^*\rho$ P-wave limits and isospin relations.

TABLE X. $\overline{K}a_1(1260)$ Branching Fractions (%), followed by the results of the isospin decomposition.

Mode	Measurement	Fit Value	BSW, with $\delta = 0 \pm 37°$
$\overline{K}^0 a_1(1260)^+$	$7.1 \pm 1.8 \pm 1.1$	$7.8 \pm 1.5 \pm 0.9$	3.8
$K^- a_1(1260)^+$	$9.0 \pm 0.9 \pm 1.7$	$8.7 \pm 0.8 \pm 1.6$	1.5 ± 0.1
$\overline{K}^0 a_1(1260)^0$	< 1.9 90% C.L.	$0.7 \pm 0.2 \pm 0.5$	0 ± 0.1
$\lvert A_{1/2}/A_{3/2}\rvert = 2.8 \pm 0.4 \pm 0.3$, $\delta = 0 \pm 21 \pm 30°$			

TABLE XI. $\overline{K}^*\rho$ Branching Fractions (%), followed by the results of the isospin decomposition.

Mode	Measurement	BSW	BSW, with $\delta = 61 \pm 37°$
$\overline{K}^{*0}\rho^+$	$4.8 \pm 1.2 \pm 1.4$	17	17
$K^{*-}\rho^+$	$6.2 \pm 2.3 \pm 2.0$	21	18 ± 3
$\overline{K}^{*0}\rho^0$	$1.9 \pm 0.3 \pm 0.7$	2	5 ± 3
$\lvert A_{1/2}/A_{3/2}\rvert = 3.4 \pm 0.7 \pm 0.7$, $\delta = 61 \pm 22 \pm 30°$			

TABLE XII. $\overline{K}_1(1270)\pi$ Branching Fractions (%), followed by the results of the isospin decomposition.

Mode	Measurement
$\overline{K}_1(1270)^0\pi^+$	< 1.1
$K_1(1270)^-\pi^+$	$1.8 \pm 0.5 \pm 0.8$
$\overline{K}_1(1270)^0\pi^0$	< 2.0
$\lvert A_{1/2}/A_{3/2}\rvert > 2.0$	

TABLE XIII. $\overline{K}_1(1400)\pi$ Branching Fractions (%), followed by the results of the isospin decomposition.

Mode	Measurement
$\overline{K}_1(1400)^0\pi^+$	$4.1 \pm 1.2 \pm 1.2$
$K_1(1400)^-\pi^+$	< 1.2
$\overline{K}_1(1400)^0\pi^0$	< 3.7
$\lvert A_{1/2}/A_{3/2}\rvert < 4.3$	

TABLE XIV. Isospin decompositions.

Mode	$\lvert A_{1/2}/A_{3/2}\rvert$	δ	$\Gamma(D^0 \to \text{Mode})/\Gamma(\text{D}^+ \to \text{Mode})$
$\overline{K}\pi^a$	3.67 ± 0.27	$77° \pm 11°$	4.8 ± 1.0
$\overline{K}\rho^a$	3.12 ± 0.4	$0° \pm 26°$	4.2 ± 1.6
$\overline{K}^*\pi^a$	3.22 ± 0.97	$84° \pm 13°$	3.3 ± 1.8
$\overline{K}a_1(1260)$	$2.8 \pm 0.4 \pm 0.3$	$0 \pm 21 \pm 30°$	3.3 ± 1.2
$\overline{K}^*\rho$	$3.4 \pm 0.7 \pm 0.7$	$61 \pm 22 \pm 30°$	4.2 ± 2.2
$\overline{K}_1(1270)\pi$	> 2.0		
$\overline{K}_1(1400)\pi$	< 4.3		

[a] Reference 6.

TABLE XV. Results from E691 on $D^+ \to \overline{K}^{*0} e^+ \nu$.

	Mark III[a]	E691[b]	ISGW[c]	BSW[d]	GS[e]	KS[f]
$A_1(0)$		$0.46 \pm 0.05 \pm 0.05$	0.8	0.9	0.8	1.0
$A_2(0)$		$0.0 \pm 0.2 \pm 0.1$	0.8	1.2	0.6	1.0
$V(0)$		$0.9 \pm 0.3 \pm 0.1$	1.1	1.3	1.5	1.0
Γ_L/Γ_T	$0.47^{+0.95+0.09}_{-0.12-0.15}$	$1.8^{+0.6}_{-0.4} \pm 0.3$	1.1	0.9	1.2	1.2

[a] Reference 9.

[b] Reference 15.

[c] Reference 33.

[d] Reference 34.

[e] Reference 35.

[f] Reference 36.

TABLE XVI. Form factors in the BSW model.

	$D \to \overline{K}^*$	$D \to \rho$
$A_1(0)$	0.88	0.78
$A_2(0)$	1.15	0.92
$V(0)$	1.23	1.23

TABLE XVII. Branching Fractions (%) in BSW model, using experimental values of form factors. The column labeled "BSW 1" lists the predictions using E691 form factors. The column labeled "BSW 2" lists the predictions using E691 form factors scaled to agree with the Mark III $D^+ \to \overline{K}^{*0} e^+ \nu$ branching fraction. Both columns assume $\delta = 61 \pm 37°$.

Mode	Measurement	BSW 1	BSW 2
$\overline{K}^{*0}\rho^+$	$4.8 \pm 1.2 \pm 1.4$	4.7 ± 1.6	8.0 ± 3.1
$K^{*-}\rho^+$	$6.2 \pm 2.3 \pm 2.0$	6.1 ± 2.3	10.4 ± 4.3
$\overline{K}^{*0}\rho^0$	$1.9 \pm 0.3 \pm 0.7$	2.1 ± 0.8	3.6 ± 1.5

TABLE XVIII. Partial wave breakdown for $\overline{K}^*\rho$ decays in BSW model.

	Amplitude			Width, 10^{10} sec^{-1}
	S-wave	P-wave	D-wave	Total
$\overline{K}^{*0}\rho^+$	$6.3a_1 + 6.4a_2$	$-1.3a_1 - 1.3a_2$	$0.9a_1 + 0.9a_2$	$34.59(a_1 + 1.04a_2)^2$
$K^{*-}\rho^+$	$6.3a_1$	$-1.3a_1$	$0.9a_1$	$34.05a_1^2$
$\overline{K}^{*0}\rho^0$	$4.5a_2$	$-0.9a_2$	$0.6a_2$	$18.45a_2^2$

FIGURE CAPTIONS

Figure 1. Recoil mass plots for the four final states being studied.

Figure 2. Invariant mass projections for the $D^0 \to K^-\pi^+\pi^+\pi^-$ final state.

Figure 3. Schematic of the $K^-a_1(1260)^+$ amplitude. The enhancement at low $K^-\pi^-$ mass is characteristic of the $K^-a_1(1260)^+$ amplitude, and is due to the longitudinal polarization of the $a_1(1260)$. The small vertical arrows indicate the polarization of the $a_1(1260)$ and ρ. The relative orbital angular momentum at each vertex is shown. To conserve angular momentum, the $a_1(1260)$ must be longitudinally polarized. Since the $a_1(1260)$ decays to $\rho\pi$ in an S-wave [37], the spin of the ρ is parallel to the spin of the $a_1(1260)$. Therefore, in the decay of the ρ, the π^- tends to be produced in a forward or backward direction with respect to the direction of the K^-, producing a distribution with an enhancement at low $K^-\pi^-$ mass.

Figure 4. The presence of the transverse $\overline{K}^{*0}\rho^0$ amplitude leads to angular correlations between $\overline{K}^{*0}$ and ρ^0 decays. (a) The $(K^-\pi^+)_1$ invariant mass. (b) A scatter plot of $(K^-\pi^+)_1$ mass vs. ϕ, where ϕ is the angle between the $\overline{K}^{*0}$ and ρ^0 decay planes as seen from the D^0 rest frame. In the $\overline{K}^{*0}$ band, an enhancement near $\phi = 0$ and a larger enhancement near $\phi = \pi$ are visible. The transverse $\overline{K}^{*0}\rho^0$ amplitude, which is proportional to $\cos\phi$, accounts for this distribution. Since the sign of this amplitude reverses from $\phi = 0$ to $\phi = \pi$, there is more constructive interference near $\phi = \pi$.

Figure 5. Scatter plots for the $\overline{K}^0\pi^+\pi^+\pi^-$ final state. (a) $\overline{K}^0\pi^-$ vs. $(\pi^+\pi^-)_2$ mass for data. (b) $\overline{K}^0\pi^-$ vs. $(\pi^+\pi^-)_{\rm high}$ mass for data. (c) $\overline{K}^0\pi^-$ vs. $(\pi^+\pi^-)_2$ mass for Monte Carlo. (d) $\overline{K}^0\pi^-$ vs. $(\pi^+\pi^-)_{\rm high}$ mass for Monte Carlo.

Figure 6. Scatter plots for the $\overline{K}^0\pi^+\pi^+\pi^-$ final state. (a) $\overline{K}^0\pi^-$ vs. $\overline{K}^0(\pi^+\pi^-)_{\rm low}$ mass for data. (b) $\overline{K}^0\pi^-$ vs. $\overline{K}^0(\pi^+\pi^-)_{\rm high}$ mass for data. (c) $\overline{K}^0\pi^-$ vs. $\overline{K}^0(\pi^+\pi^-)_{\rm low}$ mass for Monte Carlo. (d) $\overline{K}^0\pi^-$ vs. $\overline{K}^0(\pi^+\pi^-)_{\rm high}$ mass for Monte Carlo.

Figure 7. Invariant mass projections for the $D^+ \to \overline{K}^0\pi^+\pi^+\pi^-$ final state.

Figure 8. Invariant mass projections for the $D^+ \to K^-\pi^+\pi^+\pi^0$ final state.

Figure 9. Scatter plot of $K^-\pi_1^+$ mass vs. $\cos\theta_{VV}$, where θ_{VV} is the angle between $(\vec{p}_{K^-} - \vec{p}_{\pi_1^+})$ and $(\vec{p}_{\pi^0} - \vec{p}_{\pi_2^+})$.

Figure 10. Invariant mass projections for the $D^0 \to \overline{K}^0\pi^+\pi^-\pi^0$ final state.

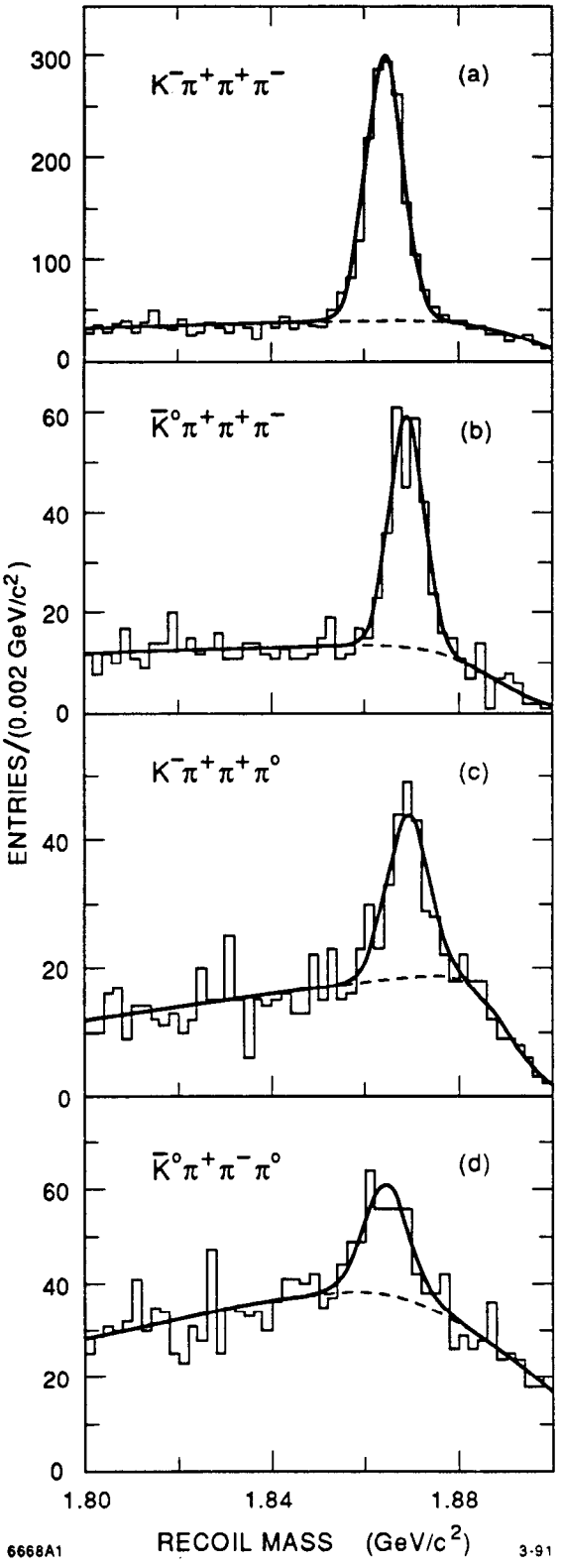
$K^-\pi^+\pi^+\pi^-$
(a)
$\bar{K}^0\pi^+\pi^+\pi^-$
(b)
$K^-\pi^+\pi^+\pi^0$
(c)
$\bar{K}^0\pi^+\pi^-\pi^0$
(d)
ENTRIES/(0.002 GeV/c^2)
RECOIL MASS (GeV/c^2)
6668A1
3-91

Fig. 1

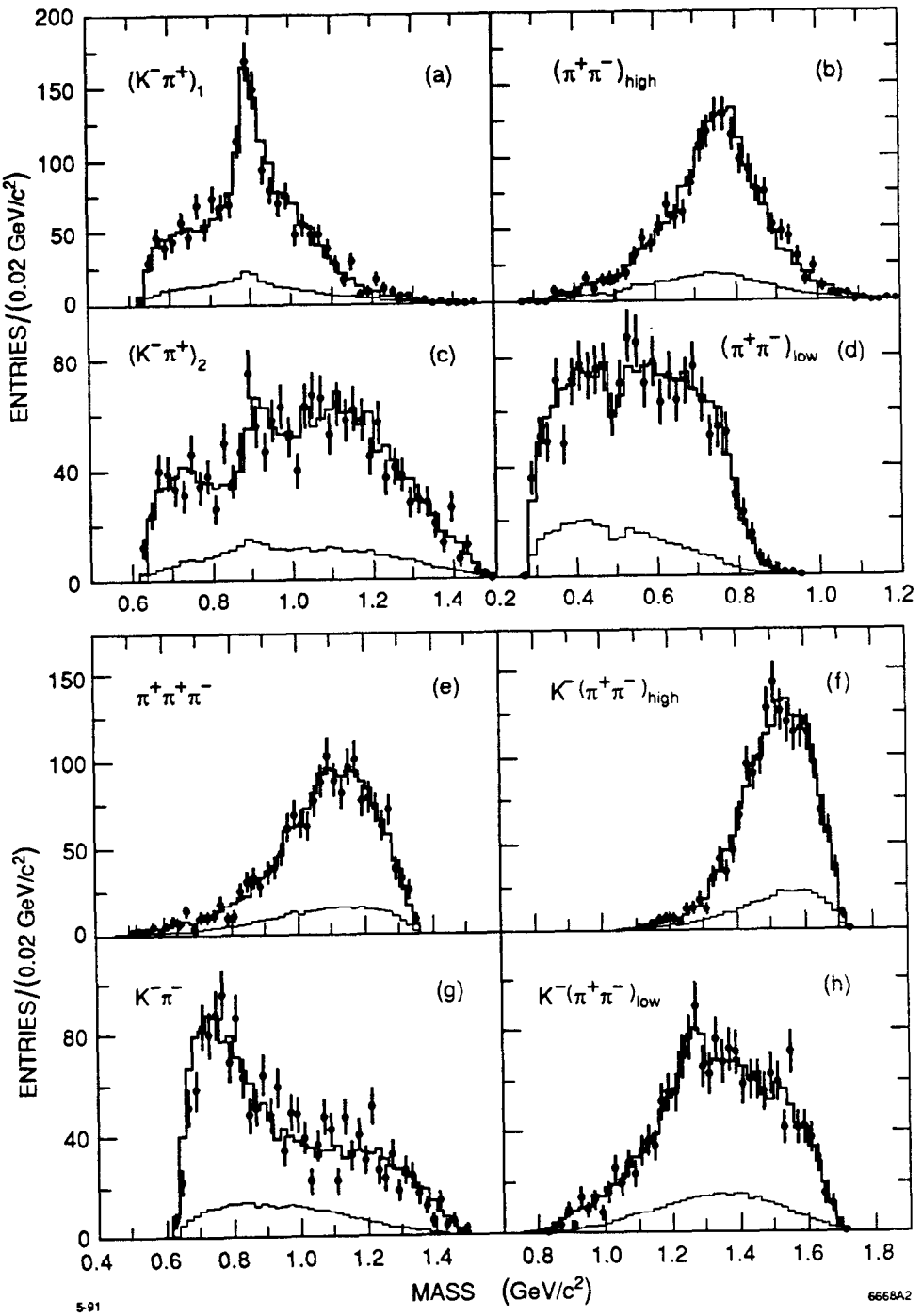
$(K^-\pi^+)_1$
(a)
$(\pi^+\pi^-)_{high}$
(b)
$(K^-\pi^+)_2$
(c)
$(\pi^+\pi^-)_{low}$
(d)
$\pi^+\pi^+\pi^-$
(e)
$K^-(\pi^+\pi^-)_{high}$
(f)
$K^-\pi^-$
(g)
$K^-(\pi^+\pi^-)_{low}$
(h)
ENTRIES/(0.02 GeV/c²)
MASS (GeV/c²)
5-91
6668A2

Fig. 2

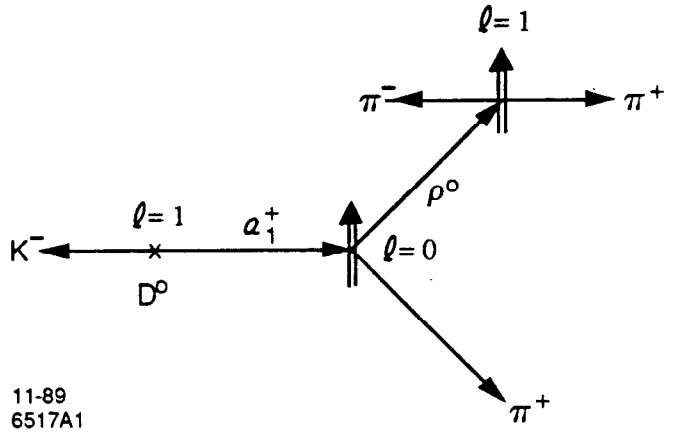

Fig. 3

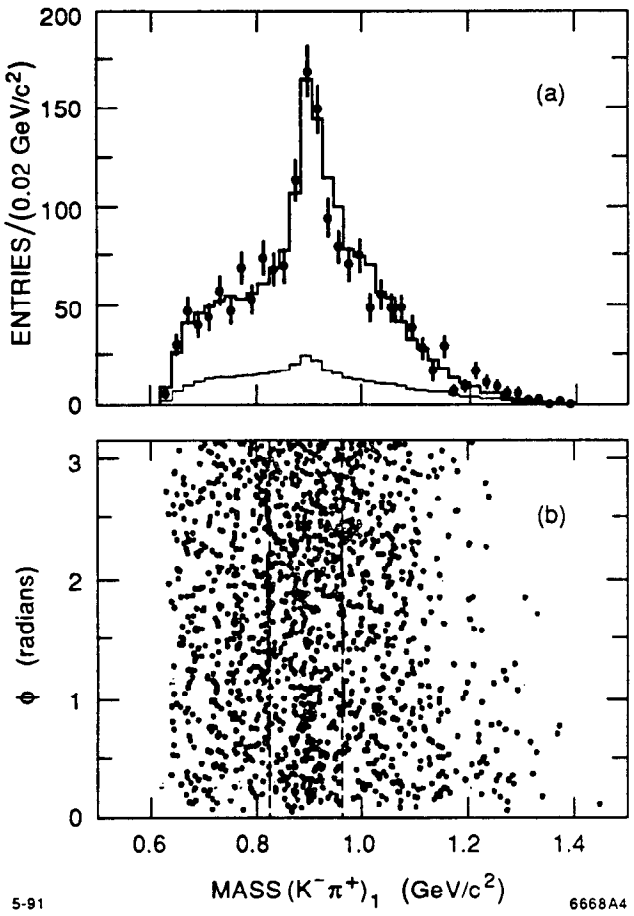
200
150
100
50
0
ENTRIES/(0.02 GeV/c²)
(a)
3
2
1
0
φ (radians)
(b)
0.6
0.8
1.0
1.2
1.4
MASS (K⁻π⁺)₁ (GeV/c²)
5-91
6668A4

Fig. 4

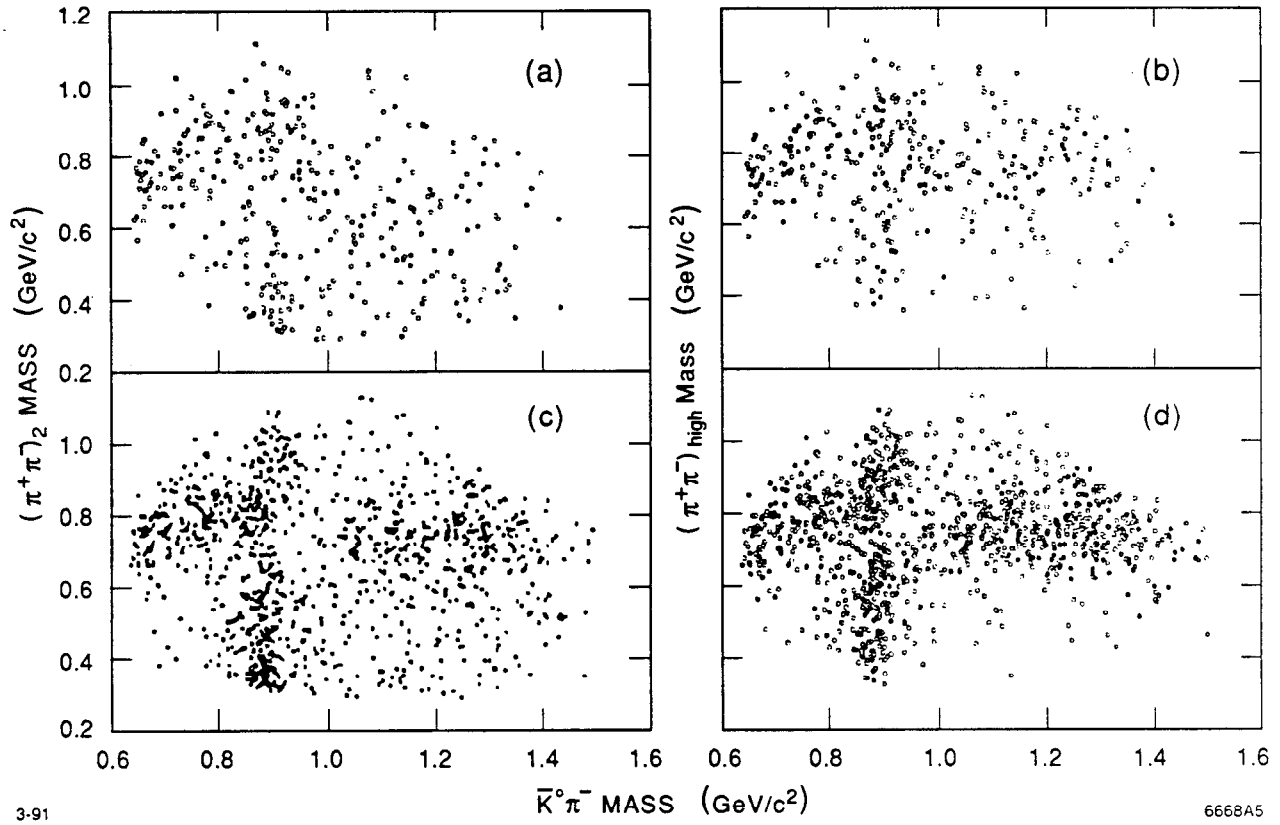
(a)
(b)
(c)
(d)
$(\pi^+\pi^-)_2$ MASS (GeV/c^2)
$(\pi^+\pi^-)_{high}$ Mass (GeV/c^2)
$\bar{K}^0\pi^-$ MASS (GeV/c^2)
1.2
1.0
0.8
0.6
0.4
0.2
0.6
0.8
1.0
1.2
1.4
1.6
3-91
6668A5

Fig. 5

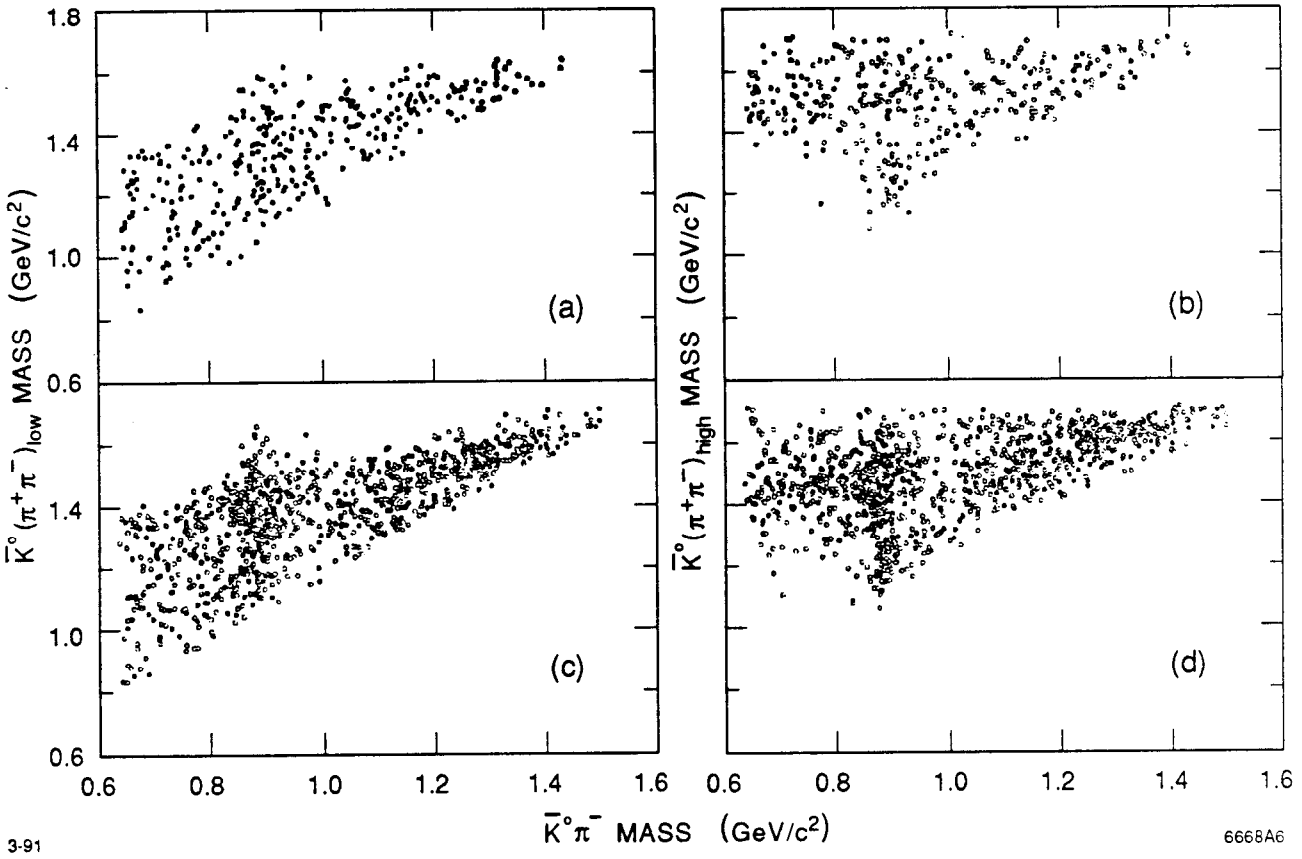
1.8
1.4
1.0
0.6
(a)
(b)
(c)
(d)
$\bar{K}^0(\pi^+\pi^-)_{low}$ MASS (GeV/c^2)
$\bar{K}^0(\pi^+\pi^-)_{high}$ MASS (GeV/c^2)
0.6
0.8
1.0
1.2
1.4
1.6
$\bar{K}^0\pi^-$ MASS (GeV/c^2)
3-91
6668A6

Fig. 6

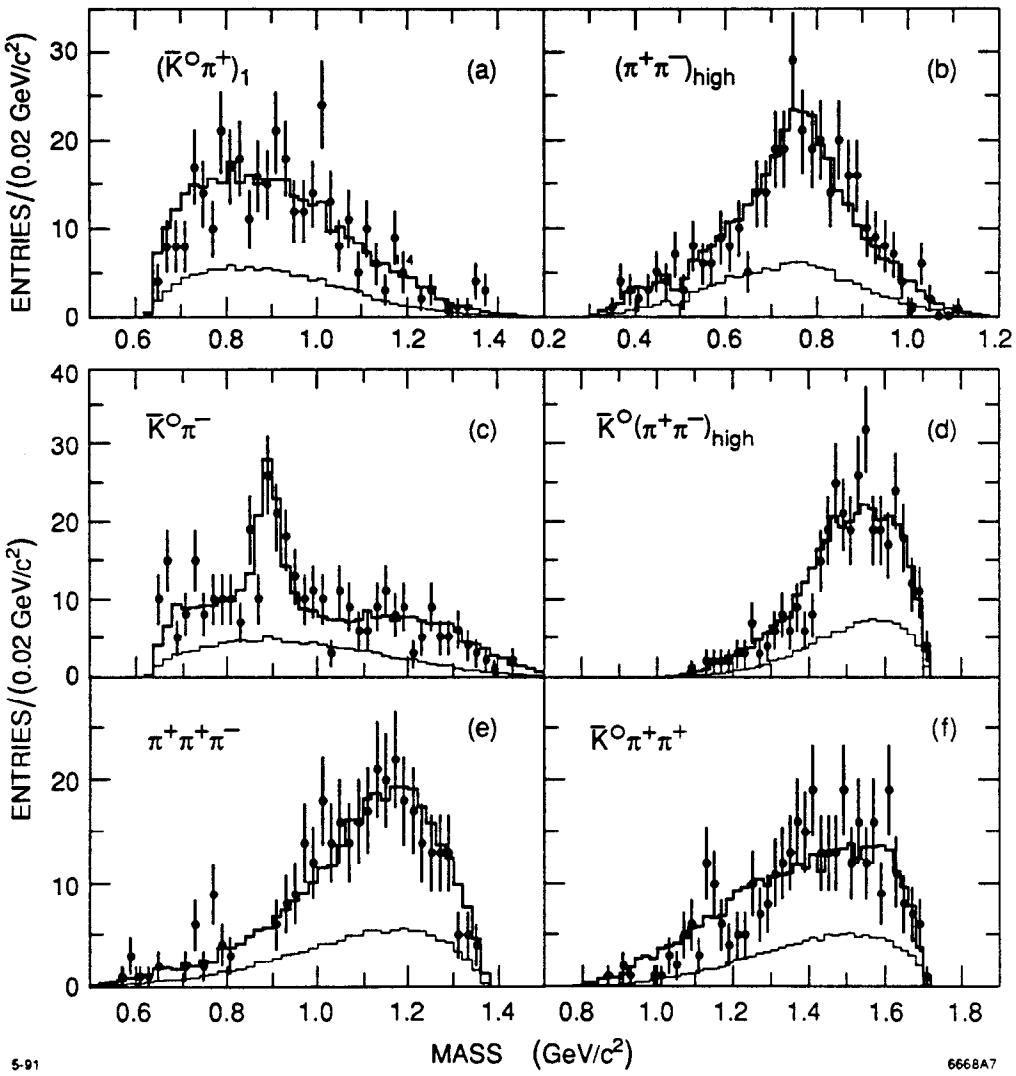
$(\bar{K}^0\pi^+)_1$
(a)
$(\pi^+\pi^-)_{high}$
(b)
$\bar{K}^0\pi^-$
(c)
$\bar{K}^0(\pi^+\pi^-)_{high}$
(d)
$\pi^+\pi^+\pi^-$
(e)
$\bar{K}^0\pi^+\pi^+$
(f)
ENTRIES/(0.02 GeV/c²)
MASS (GeV/c²)
5-91
6668A7

Fig. 7

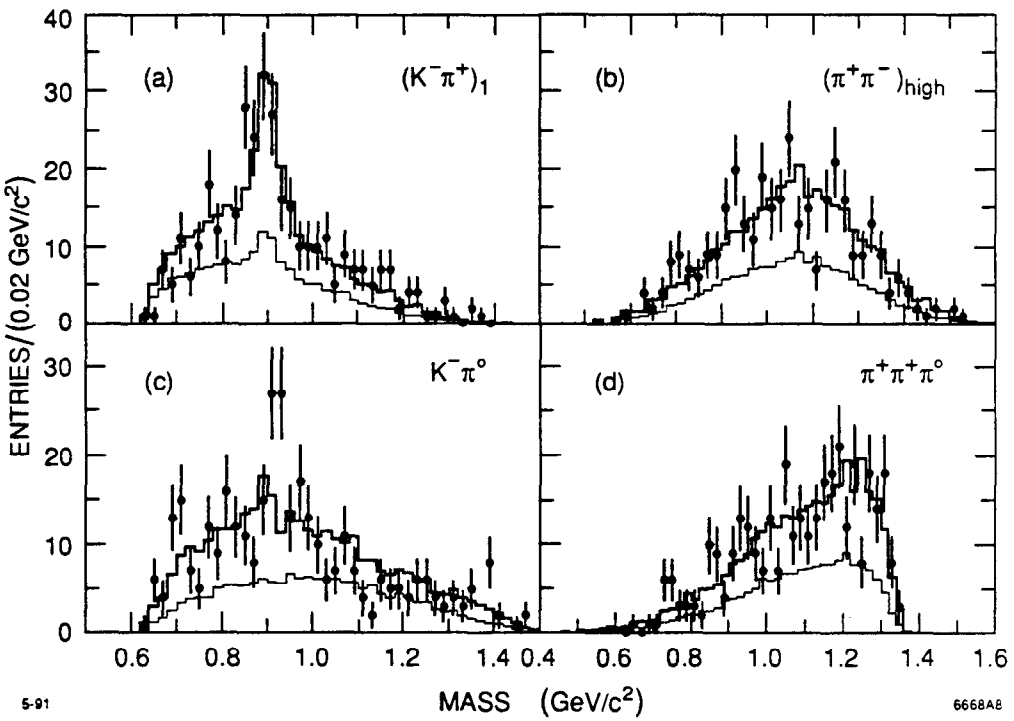
(a)
$(K^-\pi^+)_1$
(b)
$(\pi^+\pi^-)_{high}$
(c)
$K^-\pi^\circ$
(d)
$\pi^+\pi^+\pi^\circ$
ENTRIES/(0.02 GeV/c²)
MASS (GeV/c²)
5-91
6668A8

Fig. 8

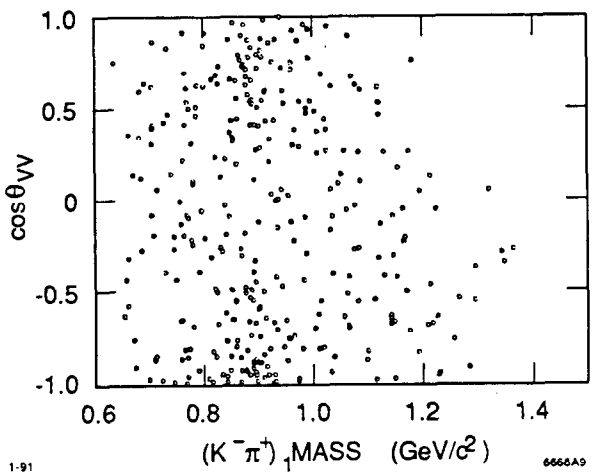
1.0
0.5
0
-0.5
-1.0
$\cos\theta_{VV}$
0.6
0.8
1.0
1.2
1.4
$(K^-\pi^+)_1$MASS (GeV/c^2)
1-91
6666A9

Fig. 9

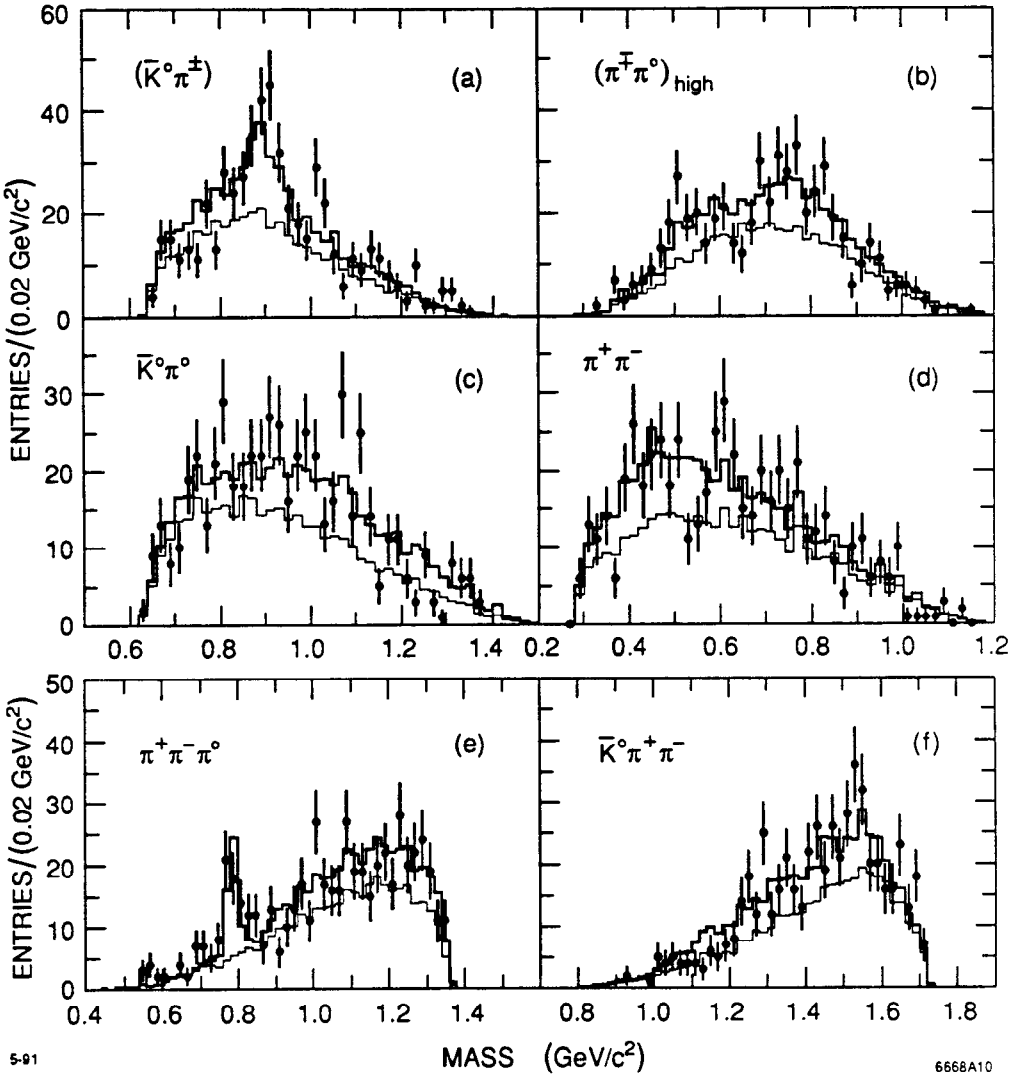
(K̄°π±)
(a)
(π∓π°)high
(b)
K̄°π°
(c)
π+π−
(d)
π+π−π°
(e)
K̄°π+π−
(f)
ENTRIES/(0.02 GeV/c²)
MASS (GeV/c²)
5-91
6668A10

Fig. 10